3D seismic imaging of the shallow plumbing system beneath the Ben Nevis Monogenetic Volcanic Field: Faroe-Shetland Basin

Charlotte E. McLean[1]*; Nick Schofield[2]; David J. Brown[1], David W. Jolley[2], Alexander Reid[3]

[1]School of Geographical and Earth Sciences, Gregory Building, University of Glasgow, G12 8QQ, UK
[2]Department of Geology and Petroleum Geology, University of Aberdeen AB24 3UE, UK
[3]Statoil (U.K.) Limited, One Kingdom Street, London, W2 6BD, UK
*Correspondence (c.mclean.1@research.gla.ac.uk)

Abstract

Reflective seismic data allows for the 3D imaging of monogenetic edifices and their corresponding plumbing systems. This is a powerful tool in understanding how monogenetic volcanoes are fed and how pre-existing crustal structures can act as the primary influence on their spatial and temporal distribution. This study examines the structure and lithology of host-rock as an influence on edifice alignment and provides insight into the structure of shallow, sub-volcanic monogenetic plumbing systems. The anticlinal Ben Nevis Structure (BNS), located in the northerly extent of the Faroe-Shetland Basin, NE Atlantic Margin, was uplifted during the Late Cretaceous and Early Palaeocene by the emplacement of a laccolith and a series of branching sills fed by a central conduit. Seismic data reveals multiple intrusions migrated up the flanks of the BNS after its formation, approximately 58.4 Ma (Kettla-equivalent), and fed a series of scoria cones and submarine volcanic cones. These monogenetic edifices are distributed around the crest of the BNS. The edifices are fed from a complex network of sills and transgressive sheets, involving lateral magma migration of tens of kilometres before extrusion at the surface. This work highlights the importance of underlying basin structures in influencing the sites and development of sub-aerial monogenetic fields, and the importance of lateral magma flow within volcanic systems.

END OF ABSTRACT

An increasing amount of evidence compiled in recent decades supports the assertion that the magma plumbing systems beneath monogenetic volcanic fields are far more complex than the dyke-dominated systems first suggested (Nemeth *et al.* 2003; Nemeth & Martin 2007; Johnson *et al.* 2008; Nemeth 2010; Brown & Valentine 2013; Re *et al.* 2015; Muirhead *et al.* 2016; Albert *et al.* 2016). Understanding the plumbing system structure beneath monogenetic volcanic fields can present significant insight into: (1) the dominant control on the distribution of individual monogenetic volcanic edifices (e.g. tectonic stress orientation vs. local crustal structure) and, therefore, assessment of the location of the next eruption centre in an active field (Buck *et al.* 2006; Le Corvec *et al.* 2013); (2) the estimated total magma volume in a system (Richardson *et al.* 2015; Muirhead *et al.* 2016); (3) the geochemical evolution of magmas and potential magma stalling/assimilation sites (Nemeth *et al.* 2003; Johnson *et al.* 2008; Smith *et al.* 2008; Albert *et al.* 2016); (4) the distance of lateral migration of magma from "source" to surface (Muirhead *et al.* 2012; Airoldi *et al.* 2016; Muirhead *et al.* 2016; Magee *et al.* 2016); and (5) controls on the emplacement mechanics and geometry of intrusions, aiding the prediction of the next eruption site (Thomson & Schofield 2008; Lefebvre *et al.* 2012; Schofield *et al.* 2012; Kavanagh *et al.* 2015; Re *et al.* 2016).

Monogenetic volcanoes are typically defined as small-volume (<0.1 km^3 dense rock equivalent total eruptive products), short-lived volcanoes that generally occur in large numbers in linear or clustered arrangements (Nemeth 2010). Geochemical analysis of monogenetic magmatic systems often assumes a vertical magmatic system, where the magma reservoir is located directly below the volcanic edifice, and does not consider the structure and spatial distribution of monogenetic plumbing systems in the shallow subsurface (Nemeth *et al.* 2003; Johnson *et al.* 2008; Smith *et al.* 2008; Kereszturi & Nemeth 2012;

Albert *et al.* 2016; Magee *et al.* 2016). The incomplete or lack of exposure of eroded plumbing systems in field studies often inhibits a full 3D analysis of monogenetic plumbing systems (Valentine & Krogh 2006; Nemeth & Martin 2007; Polteau *et al.* 2008; Schofield *et al.* 2012; Muirhead *et al.* 2012; Re *et al.* 2015; Magee *et al.* 2016; Muirhead *et al.* 2016). Reliance on geochemical analysis and inadequate field exposures can sometimes prevent a comprehensive assessment of the intrusion characteristics, magma interaction with crustal structures and, spatial and temporal development of shallow plumbing networks beneath monogenetic volcanic fields from being developed (Muirhead *et al.* 2016).

Improved imaging in reflective seismic data of magmatic plumbing systems, particularly in the last 15 years, has significantly enhanced our understanding of shallow sill complexes, their relationship to overlying magmatic vent structures, and the development of monogenetic volcanic fields (Bell & Butcher 2002; Schofield *et al.* 2012; Jackson 2012; Magee *et al.* 2013; Schofield *et al.* 2015; Magee *et al.* 2016). Using a seismic dataset from the north of the Faroe-Shetland Basin (FSB) (the Ben Nevis dataset), we examine an aligned monogenetic volcanic field and its direct relationship to the plumbing system in the subsurface. This seismic dataset allows for an assessment of the complex multi-level plumbing network, the morphology of the intrusions, and the connectivity of the monogenetic plumbing systems beneath the volcanoes.

A significant outcome of this data is the observation that the underlying structure of the basin can strongly influence the distribution of monogenetic edifices. The dataset encompasses the Ben Nevis Structure (BNS), a complex anticlinal structure covering an area of 300 km^2 (Fig. 1B, C). It should be noted that the structure is so called due to its morphological similarity, rather than any geological reason, to the topographic dome of the Ben Nevis Mountain, located on the NW Scottish mainland. This contribution provides an explanation for the presence and timing of the uplift of the Ben Nevis Structure and its

77 interdependent association with local and regional magmatic activity along the Atlantic
78 Margin.

79 Although this study focuses on one extinct monogenetic volcanic field, its findings have
80 implications for our global understanding of the plumbing systems beneath monogenetic
81 volcanic fields and the effects of the local crustal structure on the distribution of
82 monogenetic volcanoes (Valentine & Krogh 2006; Valentine & Perry 2007; Le Corvec *et al.*
83 2013; Hernando *et al.* 2014). The significance of lateral offset shallow plumbing systems
84 consisting of a network of sills, dykes and inclined sheets, has implications for the
85 geochemical and petrological signature of magma erupted from monogenetic volcanoes
86 (Magee *et al.* 2016). In addition, this study, and studies like it, can provide significant
87 information for volcanic risk to urbanised areas and infrastructure that are present within
88 active monogenetic fields (e.g. Mexico City, Mexico and Auckland, New Zealand), for
89 example, uplift and overburden deformation due to the lateral emplacement of intrusions
90 pre-eruption.

91 **Geological Background**

92 *Geological History of the FSB*

93 The Faroe-Shetland Basin (FSB) is a hydrocarbon producing basin between NW Scotland
94 and the Faroe Islands (Fig. 1), NE Atlantic. The FSB is a collective name given to a series of
95 NE-SW trending sub-basins, formed during rifting events post-Caledonian Orogeny (*ca.* 390
96 Ma) (Ebdon *et al.* 1995). The regional orientation of maximum horizontal compressional
97 stress is largely NW-SE (Holford *et al.* 2016). The FSB is characterised by intra-basinal highs
98 (Rona, Flett, Westray and Corona ridges; Fig. 1A) separating half-grabens that contain
99 accumulations of Jurassic and Cretaceous sedimentary rocks (up to 6 km) blanketed by
100 Palaeocene to Recent sediments (Naylor *et al.* 1999; Moy & Imber 2009). The initiation of

rifting of the North Atlantic in the Early Palaeocene, and the speculated impingement of a deep mantle plume, instigated magmatic activity, producing extensive lava fields, widespread ash horizons and large intrusive complexes, comprising a network of sills, connected by sub-vertical dykes and inclined sheets (White 1989; Smallwood *et al.* 1999; Smallwood & White 2002; Ellis & Stoker 2014). Large volcanic centres, that predate the rifting-associated volcanism, are identified in the northern FSB and in the Rockall, West of Scotland by large isostatic gravity and positive, circular free-air anomalies (Passey & Hitchen 2011) (Fig. 1C). The initial volcanic activity occurred at ca. 62 Ma (mid-Thanetian) and extended into the Early Eocene (Dore *et al.* 1997; Naylor *et al.* 1999; Smallwood & White 2002; Schofield *et al.* 2015). The volcanic activity produced a thick flood basalt sequence covering an area of 120,000 km^2 (Passey & Jolley 2008). The lava series is up to 5,000 m thick on the Faroe Islands and thins to the SE (Waagstein 1988; Passey & Jolley 2008). The Faroe-Shetland Escarpment (Fig. 1A, B) marks the palaeo-shoreline-shelf transition where subaerial lavas entered water, producing prograding foresets of hyaloclastite-pillow breccias and migrating the palaeo-shoreline seaward (Wright *et al.* 2012).

NW-SE trending lineaments are recognised in the FSB, cross-cutting the continental shelf (Fig. 1A) (Rumph *et al.* 1993; Lamers & Carmichael 1999; Moy & Imber 2009; Ritchie *et al.* 2011; Schofield *et al.* 2015). The origins of these lineaments are unclear, however, hypotheses include reactivated Pre-Cambrian shears (Knott *et al. 1*993) and oblique extension features formed as a response to Mesozoic rifting (Rumph *et al.* 1993). The lineaments are an important feature in controlling basin segmentation, the location of transfer zones, the source input direction and distribution of Palaeocene and Eocene sediments, and possibly controlling the input and distribution of magma in the FSB in respect to intra-basinal highs (Schofield *et al.* 2015), including the various volcanic centres (Rumph *et al.* 1993; Archer *et al.* 2005; Moy & Imber 2009; Muirhead *et al.* 2015). Post-rifting

126 subsidence and later Oligocene-Miocene localised compression resulted in minor folding of
127 Palaeocene lavas in the FSB and deposition of marine sediments (Doré & Lundin 1996;
128 Ritchie *et al.* 2003).

129 *The Ben Nevis Structure: Hydrocarbon Exploration History*

130 The Ben Nevis Structure (BNS), which forms a broad anticlinal 4-way dip-closed structure,
131 is located 15 km SE of a large Bouguer anomaly referred to as the Brendan's Volcanic
132 Centre (BVC) (Fig. 1C). The BNS is unconformably overlain by a sequence of extrusive
133 Palaeogene basaltic rocks and the Early Eocene monogenetic field, and was drilled by Shell
134 (and partners) in 2003 (Fig. 2). The pre-drill prognosis was a series of alternating
135 Cretaceous shales and sands, however, upon drilling this prognosis was found to be
136 incorrect. The BNS was dominated by Cretaceous (Maastrictian and Campanian) mudstone
137 sequences intruded by a series of Palaeogene dolerite intrusions (Fig. 2). The intrusions gave
138 rise to a series of high amplitude reflections that had been wrongly interpreted in the pre-
139 drill prognosis as potential sandstone-reservoir/mudstone-seal pairs, in an almost identical
140 scenario to a well drilled in 1997 in the Rockall Trough ("Dome Prospect") (Archer *et al.*
141 2005).

142 **Methods**

143 Acoustic impedance is the product of seismic velocity and density of a rock (Niedell 1979).
144 The high acoustic impedance between igneous material (intrusions, lavas, tuffs) and the
145 surrounding sedimentary host-rock allows for good imaging of igneous features (Smallwood
146 & Maresh 2002; Bell & Butcher 2002; Schofield *et al.* 2015). Intrusions, in particular, are
147 easily identified due to their lateral discontinuity with host-rock, high amplitude seismic
148 reflectors and are laterally limited (Thomson & Schofield, 2008). The 3D data is a time
149 migrated, zero-phase with European polarity, seismic reflection survey. The inlines and

150 cross-lines are oriented NW-SE and NE-SW respectively, with spacings of 25 m between
151 inlines and crosslines. Red reflectors indicate a 'hard' impendence response. Significant
152 horizons were picked in detail to constrain the basin structure and are shown in Fig. 2,
153 including top volcanic and base volcanic (red/brown), top of the Cretaceous (BNS) (grey),
154 sills (green) and the Balder Formation, a formation containing multiple tuff horizons (yellow).
155 It is important to note that due to the depth of the BNS (>2000 m) (low seismic
156 resolution) and overlying basalt cover, imaging of individual intrusions less than *c.* 40 m thick
157 is unlikely (Schofield *et al.* 2015). Schofield *et al.* (2015) suggest that due to the depth of
158 many sills within the contemporaneous basin fill of the FSB, seismic data can omit up to *c.* 88%
159 of the sills within a basin and therefore capturing the full complexity of the sill complex can
160 be difficult, although major magma conduits can be assessed.
161 Using 3D volume visualisation techniques, such as opacity rendering, the morphology of
162 the key volcanic features are constrained. Opacity rendering allows the transparency of
163 particular amplitudes to be individually controlled, which is highly effective when considering
164 mafic igneous bodies, as they tend to demonstrate much higher acoustic impendence than
165 the surrounding rock (Bell & Butcher 2002; Schofield *et al.* 2015). Spectral decomposition is
166 also used. This imaging technique uses frequency domains to image time-thickness variability
167 of seismic reflectivity data (McArdle & Ackers 2012). Application of this technique, which
168 produces enhanced images of the subsurface, has recently been useful in analysing volcanic
169 vents and lava distribution patterns in the FSB (Schofield & Jolley 2013; Wright 2013).

170 **Seismic observations and interpretations**

171 To better understand the distribution of the monogenetic volcanic field above the BNS, we
172 first need to understand the temporal evolution of the subsurface structure and its influence
173 on the dispersal of volcanic edifices.

Brendan's Volcanic Centre (BVC) and regional stratigraphy

A regional gravity anomaly map shows the centre of a large (c. 50 km), positive Bouguer gravity anomaly (+80mGal) in the northeastern FSB, identified as the Brendan's Volcanic Centre (BVC) (Passey & Hitchen, 2011) (Fig. 1C). The anomaly is interpreted as a result of a large magmatic body intruded at depth, however, equally a collection of smaller igneous intrusions could give rise to a singular gravity anomaly due to their proximity to each other and the low resolution of the geophysical data. The BVC is situated along one of the NW-SE trending lineaments, the Brendan's Lineament, which likely controls the site of the igneous centre (Fig. 1A) (Archer *et al.* 2005).

The lithostratigraphy in the Ben Nevis (219/21-1) and Lagavulin (217/15-1z) wells have been extrapolated across a newly acquired regional line in Figure 3, constraining the stratigraphy across the northern margin of the FSB (Fig. 4). Onlapping onto the BNS from the west is a sequence of T38 – T31 sedimentary rocks (Sullom-Lamba Formation), locally intruded by sills (Fig. 3 and 4). This T38 - T31 sequence is onlapped from a westerly direction by a sequence of T40 volcanic rocks (Flett Formation) (Fig. 4). The T40 volcanic package thickens towards the Lagavulin prospect and is comprised of tabular lavas, volcaniclastics and hyaloclastites (Millett *et al.* 2015) (Fig. 3). The T36 lava field (Lamba Formation), which is situated around the BNS, is also discretely onlapped by the T40 flows. The T36 lava field is a Kettla Member-correlative (a regional ash horizon marker) and is age equivalent to a number of small-scale rift flank volcanoes and associated lava fields in the Northern Foula Sub-basin (208/21-1) and in the Judd Sub-basin (204/28-1) (Schofield *et al.* 2015) (Fig. 1). The T36 lava field (and age-equivalent volcanic rocks in the FSB) marks the onset of widespread volcanism in the basin ca. 58.4 Ma (Schofield *et al.* 2015).

The Ben Nevis Structure (BNS) and Thanetian volcanic rocks

The BNS is situated 15 km SE of the centre of the Bouguer anomaly of the Brendans Volcanic Centre (Fig 1C). The BNS is defined by several high amplitude reflectors, that record a series of sills intruded into the Cretaceous stratigraphy, and which delineate the morphology of the anticlinal 4-way dip-closed structure (Fig. 2). The sills are generally laterally extensive for tens of kilometres within the structure and are likely concordant to the bedding of the Cretaceous stratigraphy (Fig. 2). The intrusions appear to exploit the Kyrre Formation in particular, allowing the boundary between the Kyrre Formation and the later Jorsalfare Formation to be more readily identified (Fig. 2). The sills along the NW flank and crest of the BNS terminate at the Upper Cretaceous-Palaeocene unconformity and are subsequently onlapped by T38 - T31 sediments and volcanic rocks (Fig. 5). The truncation of sills demonstrates that the sills were in place prior to the uplift, erosion and creation of the Upper Cretaceous angular unconformity. Surrounding wells to the east of the BNS (219/20-1, 219/27-1 and 219/28-2Z; Fig. 1) record between 262 m and 317 m of Selandian-aged stratigraphy (Lista Formation, Fig. 4). However, across the crest of the BNS, the Lista Formation, or equivalent Vaila Formation (Fig. 4), are absent and the T36 lava field (*ca.* 58 Ma) directly overlies the Upper Cretaceous unconformity. At the top margin of the anticline, sills are offset by normal faults, defining rotated ~1 km across fault blocks in the Jorsalfare Formation (Fig. 2). Normal faulting is also evident within the Kyrre Formation (Fig. 2).

Above the unconformity, the T36 lava field (*c.* 270 m thick) is represented on the seismic data by a series of bright, hard-kick reflectors that are relatively smooth and laterally continuous (Fig. 6). The T36 volcanic sequence generally thickens towards the NW from a few tens of metres in the SE to hundreds of metres in the NW. From well data, the lava sequence is divided by a thin, seismically unresolved shale unit (18.6 m thick) into an upper and lower lava sequence (Fig. 2). The lower lava sequence is organised in a series of low-

222 angle dipping reflectors separated by disorganised reflector packages (Fig. 6). In contrast, the
223 upper lava sequence is characterised by laterally continuous, flat reflectors. The Faroe-
224 Shetland Escarpment (FSE) (~200 – 300 m high) marks the NW margin of the Erlend Sub-
225 basin (Fig. 1 and 6). The FSE is reflected by a change in seismic responses over the scarp
226 from continuous reflectors to a series of prograding foresets characterised by highly
227 disorganised, bright reflector packages over the scarp (Fig. 6A). The reflector package
228 thickens over the FSE but thins out into the basin (Fig. 6A).

229 The thickness of the Shetland Group on either side of the BNS is also markedly
230 different (Fig. 2). The thickness of the Shetland Group is exclusively related to the thickness
231 of the overlying volcanic succession (e.g. a reduced Upper Cretaceous strata underlies a
232 thick volcanic succession).

233 *The Ben Nevis Monogenetic Volcanic Field (BNVF) and plumbing system*

234 The seismic data reveals a series of well-preserved monogenetic volcanic edifices (up to 10
235 possible edifices), primarily located on the top surface (~1900 ms to 2300 ms) of the T36
236 lava field (Fig. 7), hereafter referred to as the Ben Nevis Monogenetic Volcanic Field (BNVF).
237 The edifices are estimated to be between ~145 m to 380 m in height, <2 km in diameter,
238 and have an estimated external slope of between 11° and 35°. The internal structure of each
239 cone is represented by ordered, discrete seismic packages and when observed on time-
240 slices (horizontal slices through data), the edifices are circular or elliptical, signifying a highly
241 organised internal structure (Fig. 7; Edifices 1,6 & 7). On several of the edifices, bright
242 seismic reflectors cap the top of the cone and extend for several kilometres (Fig. 7; Edifice
243 6). Edifices 8 and 9 are present in the Erlend Sub-basin along the Faroe-Shetland Escarpment
244 (Fig. 7; Edifice 9). These edifices (8 and 9) are represented by an internal chaotic zone
245 beneath bright reflectors and are typically steep sided with a large central crater (Fig. 7;
246 Edifice 9).

247 The edifices are underlain by vertical zones of reflector discontinuity (<2 km) that
248 appear to connect with the lateral tips of very high amplitude reflectors, identified as sills
249 (Fig. 7; Edifices 1,6 and 7). The sills appear to feed upwards into these conical zones of
250 disruption and terminate. The clear spatial connection between edifice and underlying sill
251 indicates that the two features are intimately related (Fig. 7 and 8). The high amplitude
252 reflectors display a complex, vertically stacked and laterally extensive series of
253 interconnected sheets and sills (Fig. 6). The sills are intruded between 4200 ms and 2500 ms
254 which equates to <500 m to 3 km beneath the monogenetic edifices at the time of intrusion
255 (based on time-depth data of well) (Fig. 8A-C). The intrusions are expressed as tuned
256 reflection packages and so thickness can only be estimated, with an estimated maximum
257 thickness of ~100 m. The intrusions are relatively small in diameter (<1–3 km). Several
258 intrusion morphologies have been identified and are shown in Fig. 8A-C, including: (A)
259 saucer-shaped intrusions composed of a concordant inner sill that transgresses upwards at
260 the margins forming a radial or bilateral geometry (Magee *et al.* 2014) (Fig. 8A); (B) climbing
261 saucer-shaped intrusions composed of a saucer-shape intrusion that is typically less
262 transgressive on one rim than another (Planke *et al.* 2005) (Fig. 8B); and (C) inclined sheets
263 comprised of reflections that are inclined and discordant to surrounding strata (Planke *et al.*
264 2005) (Fig. 8C). The majority of the saucer-shaped and half-saucer shaped intrusions are
265 located beneath the Erlend Sub-basin (Fig. 8D). The high amplitude reflectors interpreted as
266 inclined sheets are located along the inclined Upper Cretaceous unconformity (Fig. 6), and
267 delineate the structure of the BNS (Fig. 8D.

268 Opacity rendered views of the seismic data enables the intrusion morphologies in the
269 subsurface to be evaluated. The intrusions are shown to consist of a series of lobes, or
270 coalesced fingers, which allow interpretation of the direction of magma migration (Hansen &
271 Cartwright 2006; Schofield *et al.* 2010; Schofield *et al.* 2012) (Fig. 8E, F). Magma lobes are

also evident on the inclined sheets and are seen climbing upwards to the base of the volcanic edifice (Fig. 8E, F).

Cone-like structures are identified near the base of the volcanic succession and are onlapped and subsequently buried by 1.5 km of volcanic rocks (later lavas and hyaloclastite) (Fig. 9A). High amplitude reflectors outline the cone edifice and an organised internal structure can be identified. On the timeslice views (plan view), these "cones" are near-circular, up to 380 m in height and <2 km in diameter. Bright reflectors are identified emanating away from the buried cones and are laterally extensive for up to *c.* 2 km (not consistently surrounding the cone), suggestive of localised lava flows (Fig. 7).

Edifice distribution

The edifices are arranged around the crest of the underlying BNS (Fig. 10A). There is an apparent ENE-WSW alignment of five edifices that lies sub-parallel to the axis of the BNS (Fig. 10). A statistical alignment analysis of the monogenetic edifices was conducted to assess the spatial relationship between the edifices in the alignment using the method of Paulsen & Wilson (2010). Best-fit ellipsoids of each of the edifices were used to determine the centroid of the edifice and a best-fit line was established. The total length of the proposed alignment is 28.42 km. The alignment can be classified into four reliability grades (A > B > C > D) by considering four factors: (1) number of edifices in alignment; (2) the orthogonal distance from the centroid of an edifice to the best-fit line; (3) spacing distances between edifices; and (4) angle of deviation from the best fit line to the long axis of elliptical edifices (Fig. 10B) (Paulsen & Wilson 2010; Bonini & Mazzarini 2010; Magee *et al*. 2015). The results of the analysis are provided in the supplementary data.

The alignment has been assigned a reliability grade of 'D' primarily due to the large spacing distances between edifices (3.36 km to 14 km) and the lack of elongate edifices. Elongate edifices (axial ratios >1.2) are useful for defining reliable regional vent alignments

297 (Fig. 10B) (Paulsen and Wilson 2010; Magee *et al.* 2015), however only two edifices in the
298 BNVF have a long-short axis ratio of >1.2. The 'D' reliability grading suggests the alignment
299 is statistically invalid on the basis of the parameters of the analysis (spacing distances,
300 elongation axis), however, there is a clear visual alignment (Fig. 10A).

301 **Discussion**

302 *Establishing the timing and mechanism of uplift of the BNS*

303 The sills at the top of the BNS structure (not feeding the BNVF) were dated using Ar/Ar to
304 an age of 55.6 ± 0.8 Ma (sequence T40; Flett Fm.) (Fig. 2; Fig 4; Rohrman 2007), however,
305 reliance on argon dating techniques in mafic systems is highly questionable due to the lack of
306 potassium in basic igneous bodies, high levels of alteration, and particularly small radiogenic
307 ^{40}Ar yields (Fitch *et al.* 1988, Archer *et al.* 2005). Conversely, it is clear from the seismic data
308 that, due to the truncation of these intrusions (Fig. 5), they were emplaced much earlier
309 than the Ar/Ar age suggests. The sills are truncated by the Upper Cretaceous unconformity
310 which is onlapped by the T38 – T31 stratigraphy (ca. 60 Ma).

311 From the absent Selantian-aged Vaila/Lista Formations (Fig. 4) above the BNS, it is
312 assumed that uplift and updoming of stratigraphy forming the BNS occurred between the
313 end of the Cretaceous and the Early Palaeocene (Danian and Selantian), *c.* 65 - 59 Ma. The
314 angular unconformity and truncation of the top of the Jorsalfare Formation and sills suggests
315 the uplift of the dome structure formed a local topographic high during the Early Palaeocene,
316 which caused significant subaerial erosion of the Cretaceous sequences (Fig. 11).

317 Vitrinite reflectance analysis from Well 219/21-1 shows 3.0% to 5.0%, in the sub-
318 volcanic BNS stratigraphy (2000 – 3000 m depth), corresponding to 220°C to 270°C
319 (Rohrman 2007). Furthermore, a reconstructed temperature history (Rohrman 2007)
320 shows a heat spike at 65–60 Ma of 90 mW/m^2 which cannot be explained by just heat

conduction from the sills (Rohrman 2007). This elevated heat signature implies that there was a deep-seated heat source directly below the BNS before the onset of Late Palaeocene volcanism (Rohrman 2007). It is therefore likely that the intrusions were emplaced synchronously with an underlying laccolith that created the mechanism for uplift (Fig. 12A). The laccolith uplifts the overburden causing forced folding that induces bedding plane slip in the overlying stratigraphy (Fig. 12B; Archer *et al*. 2005). The sills exploit the weakness in the bedding planes during early inflation of the pluton creating stacked sills that emanate from the larger body (Fig. 12B; Archer *et al.* 2005). Continuous doming caused by inflation of the laccolith is assisted by the inflation of the sills, producing a significant amount of updoming of the overburden. Both magmatic events (laccolith and associated intrusions) caused significant heating of the Upper Cretaceous stratigraphy (Fig. 12A).

In the Rockall Basin, 530 km to the SW (Fig. 1), a similar structure to the BNS is recorded in the Cretaceous stratigraphy (Archer *et al.* 2005). The intrusions forming the Rockall Dome Structure were dated to 63.3 Ma to 64.2 Ma using Ar/Ar in biotite, a much more reliable dating source (Archer *et al.* 2005). The occurrence of very similar structures in the Danian approximately 530 km apart suggests a potential regional magmatic event in the Late Cretaceous/Early Palaeocene across the NE Atlantic Margin. Furthermore, this magmatic episode (around *c.* 63-64 Ma) appears to be focussed along NW-SE trending lineament structures (Brendan's Lineament and Wyville Thomson Lineament Complex; Fig. 1) and/or transfer zones, and may appear elsewhere along the North Atlantic Margin.

Effect of the BNS palaeo-high on T36 volcanic rocks

During the Late Palaeocene, the uplifted BNS was exposed subaerially forming a broadbacked palaeo-high (Fig. 11). By assessing the original height of the BNS, it is estimated that up to 700 m of eroded material was removed from the top of the BNS. Differential compaction of the Cretaceous stratigraphy occurred on either side of this palaeo-high due

346 to the variable thickness of the overburden (volcanic succession) (Smythe *et al.* 1983; Passey
347 & Hitchen 2011). Sediment accumulation in the west increased compaction and subsidence
348 of the Cretaceous strata, forming accommodation space on the west side of the BNS, which
349 filled with T38–T31 sediments, hyaloclastite packages and later lavas (T40), represented on
350 the seismic as bright reflectors onlapping the top Cretaceous unconformity (Fig. 3 and 11).
351 It is likely the lack of T38-T31 sediments on the east side of the BNS is partially depositional,
352 however, sagging onlap reflectors on the west margin of the BNS (Fig. 5) provide evidence
353 that subsidence occurred synchronously with deposition, which is not evident on the east
354 margin.

355 Eruption of the T36 lava field (*ca.* 58.4 Ma) was likely sourced from localised, rift-
356 flank volcanoes similar to other T36 lava fields, for example in the Northern Foula Sub-basin
357 and the Judd Basin (Schofield *et al.* 2015). By assessing the thickness of the volcanic
358 succession (thickens towards the NW), the source of the lavas are expected to be NW of
359 the dataset. The BNS palaeo-high prevented the earliest lava flows in the T36 lava field from
360 advancing towards the east. Subsequent lava flows were able to breach the palaeo-high and
361 flowed towards the east and the FSE (Fig. 11). A change in seismic responses over the FSE
362 (Fig. 6) are attributed to shallow hyaloclastite deltas fed by the lavas and are indicative of
363 where subaerial lavas entered the Erlend Sub-basin (Naylor *et al.* 1999; Passey & Hitchen,
364 2011). Small-volume lavas produced by the BNVF edifices add to the complexity of the lava
365 field.

366 *Ben Nevis Monogenetic Volcanic Field (BNVF) and underlying plumbing system*

367 The plumbing system and linking to edifices

368 In the Late Palaeocene/Early Eocene, the Cretaceous stratigraphy in the NE Erlend Sub-basin
369 was heavily intruded by an extension of the Faroe-Shetland Sill Complex (FSSC) (Bell &

370 Butcher 2002; Passey & Hitchen 2011; Schofield *et al.* 2015), comprising >130 resolvable
371 saucer-shaped and half-saucer-shaped intrusions (Fig. 8). The FSSC is part of a wider
372 complex of sills across the North Atlantic Margin (Schofield *et al.* 2015). The intrusion of
373 these sills is thought to have occurred relatively synchronously across this margin around 55
374 Ma, however, earlier magmatic phases are reported throughout the FSB, beginning from the
375 Late Cretaceous through to Flett Formation times (55.2 Ma) (Schofield *et al.* 2015).

376 During the emplacement of the sill complex, as magma encountered the BNS, the
377 magma appears to have exploited the Upper Cretaceous unconformity and the boundary
378 between the Jorsalfare and Kyrre Formations (Fig. 8). Mechanical contrasts across these
379 boundaries creates conditions that promote intrusion parallel to bedding (Kavanagh et al.
380 2006). This channelled magma to the surface, resulting in inclined sheets intruding up the
381 flanks of the dome structure feeding edifices around the crest of the underlying BNS on the
382 contemporaneous surface (Fig. 10A). Alignment analyses suggest the alignment
383 corresponding to the northern flank of the BNS crest is statistically invalid (Fig. 10B). More
384 statistically reliable (hydrothermal and magmatic) vent alignments tend to form in response
385 to magma (or hydrothermal fluids) exploiting faults, if magma exploits along the entire fault
386 length (Paulsen & Wilson 2010; Bonini & Mazzarini 2010; Magee *et al.* 2015). Magee et al.
387 (2015) suggest the convex-upwards, upper tip-line geometry of faults can direct fluids to the
388 fault centre, locally limiting hydraulic failure of the overburden and localizing vent
389 distribution along the fault trace. This effective channelling of magma does not occur as
390 efficiently beneath the BNVF as the magma exploits bedding planes, not faults, which results
391 in a less definitive alignment due to the irregular structure of the underlying anticline (BNS).

392 Conical zones of disruption are identified in seismic data between the feeder sills and
393 some of the edifices in the BNVF (Edifice 1 in Fig. 7). This feature is commonly found
394 beneath all vent/mound types (e.g. hydrothermal, sediment and magmatic) (Bell & Butcher,

2002; Svensen *et al.* 2006; Grove 2013 Magee *et al.* 2014; Galland *et al.* 2014; Jackson 2012; Manton 2015) and may represent: (i) vertically mobilised sediment induced by hydrothermal fluids around sills (Grove 2013); (ii) the migration of phreatic fluids (hydrothermal complexes) (Svensen *et al.* 2006); (iii) phreatomagmatic diatreme structures formed by several hundred phreatomagmatic explosions in the subsurface (White & Ross 2011); and (iv) dense, magmatic feeder dykes. In the case of the BNVF, disrupted zones beneath edifices most likely represent abundant feeder dykes due to the magmatic nature of the edifices.

Monogenetic volcanic edifices

The formation of the BNVF was contemporaneous with the T36 lava field suggesting that the intrusions feeding the BNVF were associated with an early phase of FSSC emplacement at *ca.* 58 Ma, near the onset of widespread volcanism in the basin (Fig 11). The majority of the monogenetic volcanic field is comprised of scoria cones, represented as constructional edifices with typically steep external slope angles and internal craters, and capped by bright reflectors reflecting individual low-volume lava flows (< 0.1 km^3; Nemeth 2010) (Fig. 7; Edifices 1,6 & 7). Using spectral decomposition, imaging of these lava flows has been obtained and individual lava flows can be mapped (Fig, 7). The edifices differ from hydrothermal vents, commonly represented as craters, mounds or eye-shaped seismic structures (Planke *et al.* 2005; Svensen *et al.* 2006; Hansen *et al.* 2008). Although hydrothermal vents are typically located above the tips of sills, like the BNVF edifices, they tend to have a disorganised internal structure and an underlying sag-like structure, representative of a subsidence-formed crater, which are not apparent beneath the BNVF edifices (Fig. 7) (Jamtveit *et al.* 2004; Svensen *et al.* 2006; Hansen *et al.* 2008). Furthermore, the internal structure of the BNVF edifices is clearly defined by high amplitude reflectors indicating a well-organised structure comprised of lavas and volcanic material (Fig. 7).

419 The edifices present on the margin of the Faroe-Shetland Escarpment (Fig. 7; Edifice
420 9) are inferred as submarine magmatic vents due to their location next to the FSE (which
421 marks the palaeoshoreline during the Late Palaeocene/Early Eocene), and their internal
422 chaotic seismic character (Fig. 7; Edifice 9). The type of submarine edifice (pillow-lava
423 dominated or hyaloclastite dominated) is determined by the water depth at point of magma
424 extrusion (Kokelaar 1986). Where water depths are greater than 130 m, vesiculation of
425 magma is suppressed and pillow lavas will be extruded typically forming low angle mounds
426 (Kokelaar 1986). At shallow water depths (<130 m), submarine fountaining of magma can
427 occur, causing intensive quenching and fragmentation of magma and the production of
428 edifices comprised of hyaloclastite, tephra, pillow lavas and reworked material (Kokelaar
429 1983). The submarine edifices (Fig. 7; Edifice 9) are steep sided with a large central crater,
430 suggesting that high rates of submarine magma fountaining (and therefore instantaneous
431 quenching and fragmentation of magma) built hyaloclastite dominated submarine volcanic
432 cones (Kokelaar 1983; Bell & Butcher 2002).

433 *Significance of sills and transgressive sheets in monogenetic plumbing systems*

434 Kereszturi & Nemeth (2012) consider lateral migration of magma to be minimal beneath
435 monogenetic fields and imply that the location of the edifice is a good approximation of the
436 location of magma source in the subsurface. The Ben Nevis seismic data indicates that
437 lateral migration of magma can occur for up to 10 km before the eruption of magma at the
438 surface (Fig. 6). Vertically extensive, stacked sill complexes (<10 km) feeding monogenetic
439 edifices, similar to the BNVF, are also recorded in the Møre and Vøring basins in offshore
440 Norway and the Ceduna Sub-basin offshore Australia (Cartwright & Hansen 2006; Jackson
441 2012; Magee *et al.* 2013; Manton 2015). Seismic imaging and field based studies of such
442 intrusion networks clearly shows sills and inclined sheets can provide the dominant magma
443 storage and transport pathway beneath monogenetic volcanic fields in primarily extensional

444 tectonic settings (and back arc extensional regimes) (Cartwright & Hansen 2006; Valentine
445 & Krogh 2006; Nemeth & Martin 2007; Jackson 2012; Kiyosugi *et al.* 2012; Muirhead *et al.*
446 2012; Magee *et al.* 2013; Magee *et al.* 2014; Re *et al.* 2015; Richardson *et al.* 2015; Magee *et al.*
447 2016; Muirhead *et al.* 2016).

448 Interrelated sills and inclined sheets at Hopi Buttes, Arizona, featuring ramped step
449 and stair, saucer-shaped and half-saucer-shaped intrusion morphologies, form at least 30% of
450 the total magma volume of the monogenetic plumbing system (Muirhead *et al.* 2016). At San
451 Rafael Monogenetic Volcanic Field, this percentage increases to 93% (Richardson *et al.* 2015).
452 An absence of dykes in the Crown Butte complex at Hopi Buttes, and the ratio between
453 magma storage in sills versus dykes at San Rafael demonstrates the significance of sills and
454 inclined sheets in transporting magma to the surface beneath monogenetic fields (Muirhead
455 *et al.* 2016). However, the total volume of magma storage in sills and transgressive sheets
456 cannot be fully elucidated by just field data due to the current level of exposure of some
457 fields, where the complex, stacked nature of the sill complexes are not fully exposed.

458 Seismic unrest studies have suggested stalling of magma in the upper crust can occur
459 up to two years before a monogenetic eruption, indicating multiple potential intrusion
460 events pre-eruption. For example, the 2011 eruption offshore of El Hierro in the Canary
461 Islands was preceded by 4-5 years of seismic unrest activity, suggestive of the development
462 of a complex plumbing system (Albert *et al.* 2016). The evidence for shallow plumbing
463 systems is further corroborated by geochemical studies which allude to the presence of sub-
464 horizontal, shallow plumbing systems where crustal assimilation, crystallization and melt
465 storage is recorded (Nemeth *et al.* 2003), especially beneath relatively long-lived scoria
466 cones such as Jorullo and Paricutin (15 yr and 9 yr respectively) in the Michoacán–
467 Guanajuato Volcanic Field of the Trans-Mexican Volcanic Belt (McBirney *et al.* 1987; Johnson
468 *et al.* 2008).

469 The BNVF demonstrates that although each individual monogenetic edifice stems
470 from a discrete magma "reservoir" or intrusion, the overall plumbing system of a volcanic
471 field can be interconnected and genetically related. Consequently, two distinct magma
472 batches feeding separate edifices can share a common plumbing system and still produce
473 different compositional trends due to the isolation of the individual feeding intrusions. In
474 other words, assimilation trends for each individual edifice may not be identical across a
475 monogenetic volcanic field but would record the trends of a separate branch of a shared
476 plumbing system.

477 *Emplacement of monogenetic plumbing systems and influence of the local crustal structure*

478 It is important to consider why sill-dominated plumbing systems form as opposed to dyke-
479 dominated systems. For sub-horizontal intrusions (including saucer-shaped sills and inclined
480 sheets) to form, two main constraints must be overcome to convert magma from a vertical
481 pathway to a horizontal one: (1) magma driving pressure must exceed host-rock strength or,
482 in this case, the tensile strength of a pre-existing plane of weakness (Valentine & Krogh
483 2006); (2) the rotation of the principal stress (sigma 1) from vertical to sub-horizontal (and
484 compressive stress, sigma 3, to a sub-vertical orientation) (Kavanagh *et al.* 2006; Valentine &
485 Krogh 2006; Menand 2008). In extensional tectonic settings the principal stress (sigma 1) is
486 vertical and the compressive stress (sigma 3) is horizontal (Anderson 1951; Burchardt 2008).
487 Unconformities or host-rock interfaces with sufficiently contrasting mechanical and
488 rheological properties (rigidity, strength, pore fluid pressure) can cause the rotation of the
489 principal stress (sigma 1) from vertical to horizontal, and can subsequently promote the
490 propagation of a sub-horizontal intrusion (Kavanagh *et al.* 2006; Menand 2008; Thomson &
491 Schofield 2008; Gudmundsson 2011; Magee *et al.* 2013; Kavanagh *et al.* 2015; Tibaldi 2015;
492 Magee *et al.* 2016). In some cases sill intrusion into a pre-existing weakness or bedding plane

493 does not require a rotation of sigma 3 to horizontal. This occurs when the sill intrudes
494 obliquely to the least compressive stress (sigma 3) (Jolly & Sanderson 1997). Horizontal or
495 sub-horizontal propagation is, therefore, a function of magma pressure, tectonic stress and
496 the strength of the weakness.

497 Compliant lithologies are exploited by magma through ductile deformation of the
498 host-rock, for example: coal (e.g. Raton Basin, Colorado, USA; Schofield *et al.* 2012); salt
499 (e.g. Werra-Fulda Basin, Germany; Schofield *et al.* 2014); and shale (e.g. Golden Valley Sill,
500 South Africa; Schofield *et al.* 2010). The mechanically weak layers can inhibit vertical crack
501 propagation, limiting vertical migration of magma and promoting horizontal migration along
502 the compliant layer (Thomson 2007; Schofield *et al.* 2012). Therefore, in thick sedimentary
503 sequences, it is likely that sill complexes will develop either by exploiting host-rock
504 interfaces in the strata, and/or by exploiting compliant horizons (Fig. 13) (Eide *et al.* 2016).

505 The abundance of saucer-shaped and half-saucer shaped intrusions in the BNVF
506 plumbing systems is likely a result of strong host-rock control and exploitation of compliant
507 horizons in the Upper Cretaceous stratigraphy (e.g. shales). In the case of the inclined
508 sheets, the magma exploited the mechanical difference along the inclined Cretaceous-
509 Palaeocene unconformity (claystones and extrusive volcanic rocks) and between the
510 Jorsalfare Formation (Fig. 14A). Due to the orientation and nature of the BNS structure,
511 these planes of weakness were inclined and supported the injection and propagation of
512 magma upwards towards the surface (whilst also contributing to lateral magma migration),
513 forming inclined sheets and dictating the location of the edifice (Fig. 14A).

514 Inclined sills have been found to be formed by various other mechanisms. The
515 formation of the inclined limbs of a saucer-shaped sill may be instigated by forced folding of
516 the overburden above a sill, where extensional fractures form near the termination of the
517 sill (Thomson 2007) (Fig. 14B). The rapid decrease in hydrostatic pressure due to the

518 opening of these fractures, instigates localised host-rock fluidisation (also caused by heating
519 of host-rock pore-fluids) (Schofield *et al.* 2010). Magma exploits these failures, propagating
520 upwards into the fluidised host-rock as a series of localised flow pathways ("magma fingers")
521 which coalesce into a singular sheet (Fig. 14B) (Thomson 2007; Schofield *et al.* 2010). The
522 "saucer" morphology is formed by radially upward-propagating magma fingers surrounding
523 an inner sill (Schofield *et al.* 2012). Field evidence for this type of structure is found at the
524 Golden Valley Sill in the Karoo Basin, South Africa, where undulations in the transgressive
525 rim, provide evidence for coalesced discrete magma pathways, or "fingers", and host-rock
526 fluidisation structures are observed surrounding magma fingers (Schofield *et al.* 2012).
527 Alternatively, transgressive sheets may also develop as a result of changes to the lithostatic
528 pressure of the host-rock environment. Re *et al.* (2015) suggest that the application or
529 destruction of a load at the surface (e.g. by the development of a volcanic edifice), or the
530 development of a diatreme, will alter the compressive stress regime (sigma 1 and 3) in the
531 host-rock strata, preventing vertical dyke propagation and resulting in an inclined magma
532 pathway (Fig. 14C).

533 Extensional monogenetic volcanic fields tend to show one or more edifice alignment
534 orientations, typically a regional stress-controlled orientation and/or alignments controlled
535 by pre-existing (dipping) crustal fractures and normal faults (Le Corvec *et al.* 2013; Magee *et*
536 *al.* 2013; Muirhead *et al*. 2015; Schofield *et al.* 2015; Mazzarini *et al*. 2016; Muirhead *et al.*
537 2016b). Pre-existing faults are known to influence the distribution of monogenetic edifices
538 depending on the fault dip angle, the orientation of the fault plane, the mechanical properties
539 of the adjacent host-rock, and the localised stress regime around the fault (Gaffney *et al.*
540 2007; Magee *et al.* 2013; Le Corvec *et al.* 2013). Basin-scale flexures in the hanging wall of
541 half-graben basins in rift settings can trigger extensional faulting and fracturing, and may also
542 control the alignment of edifices (Muirhead *et al.* 2016b). The BNVF consistently

543 demonstrates just one vague alignment orientation (corresponding to the crest of the BNS
544 structure; Fig 10). This ENE-WSW alignment of edifices contradicts the regional stress
545 orientation (NW-SE) (Holford *et al.* 2016) and no fault pathways have been identified on the
546 seismic data (although potential faults could be obscured by the poor sub-basalt imaging). As
547 a result, we suggest that the primary influence on edifice distribution in the BNVF is the
548 inclined rheological boundaries in the subsurface strata. Magma interaction with local crustal
549 structures (e.g. folds, inclined rheological boundaries), has been significantly overlooked as a
550 dominant influence over the distribution of monogenetic edifices but should be considered
551 when assessing future eruption sites of active monogenetic fields.

552 *Reactivation of magma migration pathways during the lifetime of a monogenetic volcanic field*

553 The observation of buried volcanic edifices beneath the BNVF (Fig. 9) gives a unique
554 perspective of the distribution of monogenetic edifices and how they are distributed spatially
555 and temporally. The offset between the buried cones and the later monogenetic edifices is
556 less than 1 km (Fig. 9). The lateral proximity between the buried cones and later edifices
557 suggests a similar magma pathway for both edifice-forming events. One example, beneath
558 Edifice 1 (Fig. 9A), shows a high amplitude reflector inclining vertically into the base of an
559 earlier cone and then transgressing further into the base of a later edifice (Fig. 9A). The
560 timescale between the emplacement of magma beneath the earlier cone (onset of lava, *ca.*
561 59 Ma) and the emplacement of magma beneath the later cone (final stages of lava field
562 development, *ca*. 58 Ma) is too long for the magma pathway to stay molten in a <80 m thick
563 intrusion at such a shallow depth (<1.5 km beneath the palaeosurface) due to high cooling
564 and crystallisation rates (Fig. 9A). It is therefore suggested that the high amplitude reflector
565 signifies multiple stacked intrusions (Fig. 9B). The majority of sills observed in seismic are
566 expressed as tuned packages of reflectors, thus making it difficult to discern whether a thick
567 bright reflector is the product of one sizable intrusion or a series of incrementally emplaced

or stacked intrusions (Magee *et al.* 2016). A newly-developed intrusion can impart a thermal, rigidity or strength anisotropy on to subsequent injections and further promote horizontal propagation of future intrusive events (Fig. 13) (Gudmundsson & Brenner 2004; Kavanagh *et al.* 2006; Menand 2008; Burchardt 2008). We interpret that after feeding the earlier (buried) cone, the sill provided a strong mechanical discontinuity between the sill and the surrounding host-rock (Annen *et al.* 2015; Magee *et al.* 2016) (Fig. 13). The new magma pulse, feeding the monogenetic edifices on the top volcanic surface, exploited this contact, stacking the intrusions and increasing the apparent thickness of the sill in seismic (Magee *et al.* 2016) (Fig. 13). This stacking of intrusions spatially and temporally can have significance for the thermal and chemical evolution of the later magma batch (e.g. slower cooling intrusions) (Annen *et al.* 2015; Magee *et al.* 2016).

Conclusions

The seismic data presented here offers an insight into how monogenetic volcanic fields are fed, and how the distribution of edifices can be primarily influenced by the structure of the substrate. This data can give an understanding of the characteristic and distribution of plumbing systems in active volcanic fields, or where ancient volcanic fields are poorly exposed in the field. The Ben Nevis seismic data adds to the growing body of evidence that monogenetic plumbing systems are far more complex than first suggested, where shallow saucer-shaped intrusions and inclined sheets form the majority of the magmatic system. Our research shows that the anticlinal Ben Nevis Structure beneath the Ben Nevis Volcanic Field significantly influenced the structure of the plumbing system and the subsequent distribution of volcanic edifices on the surface. Magma exploited the distinctive rheological boundary along the inclined Upper Cretaceous unconformity and between the Jorsalfare and Kyrre Formations, and fed an indefinite alignment of edifices along the axis of the BNS. The plumbing system beneath the BNVF is characterised by an intricate overlapping series of

593 saucer-shaped sills, half-saucer shaped sills and inclined sheets, which are connected by
594 seismically unresolvable feeder dykes, over a vertical thickness of ~3 km. These intrusions
595 are connected to a series of scoria cones and submarine volcanic cones. Vertically-stacked
596 edifices suggest that magma pathways in the subsurface are exploited multiple times during
597 the lifetime of a volcanic field.

598 We suggest that the sill-dominated plumbing system, seen beneath the Ben Nevis
599 Monogenetic Volcanic Field, is present beneath other monogenetic volcanic fields. Further
600 work is required to use this study, and others like it, to aid the forecasting of magma
601 migration beneath active fields, and produce accurate hazard assessments of the next
602 eruption site.

603 **Acknowledgements**

604 This work was completed as part of CM's PhD research, funded by a College of Science and
605 Engineering PhD scholarship at the University of Glasgow. Statoil are thanked for providing
606 the Brendans Dome 3D volume. PGS are thanked for donation of the CRRG 2D
607 GeoStreamer® data used in Figure 3. Seismic interpretation was carried out at University of
608 Aberdeen using IHS Kingdom Software and FFA Geoteric. Craig Magee and an anonymous
609 reviewer are thanked for positive and helpful reviews of the manuscript.

610 **References**

611 Airoldi, G. M., Muirhead, J. D., Long, S. M., Zanella, E., & White, J. D. (2016). Flow dynamics
612 in mid-Jurassic dikes and sills of the Ferrar large igneous province and implications
613 for long-distance magma transport. Tectonophysics, 683, 182-199.

614 Albert, H., Costa, F., & Martí, J. (2016). Years to weeks of seismic unrest and magmatic
615 intrusions precede monogenetic eruptions. Geology, 44(3), 211-214.

616 Anderson, E. M. (1951). The dynamics of faulting and dyke formation with applications to
617 Britain. Hafner Pub. Co..
618 Annen, C., Blundy, J. D., Leuthold, J., & Sparks, R. S. J. (2015). Construction and evolution of
619 igneous bodies: Towards an integrated perspective of crustal magmatism. Lithos, 230,
620 206-221.
621 Archer, S. G., Bergman, S. C., Iliffe, J., Murphy, C. M., & Thornton, M. (2005). Palaeogene
622 igneous rocks reveal new insights into the geodynamic evolution and petroleum
623 potential of the Rockall Trough, NE Atlantic Margin. Basin Research, 17(1), 171-201.
624 Bell, B., & Butcher, H. (2002). On the emplacement of sill complexes: evidence from the
625 Faroe-Shetland Basin. Geological Society, London, Special Publications, 197(1), 307-
626 329.
627 Bonini, M., & Mazzarini, F. (2010). Mud volcanoes as potential indicators of regional stress
628 and pressurized layer depth. Tectonophysics, 494(1), 32-47.
629 Brown, R. J., & Valentine, G. A. (2013). Physical characteristics of kimberlite and basaltic
630 intraplate volcanism and implications of a biased kimberlite record. Geological
631 Society of America Bulletin, 125(7-8), 1224-1238.
632 Buck, W. R., P. Einarsson, and B. Brandsdóttir (2006), Tectonic stress and magma chamber
633 size as controls on dike propagation: Constraints from the 1975–1984 Krafla rifting
634 episode, J. Geophys. Res., 111, B12404, doi:10.1029/2005JB003879.
635 Burchardt, S. (2008). New insights into the mechanics of sill emplacement provided by field
636 observations of the Njardvik Sill, Northeast Iceland. Journal of Volcanology and
637 Geothermal Research, 173(3), 280-288.
638 Cartwright, J., & Hansen, D. M. (2006). Magma transport through the crust via
639 interconnected sill complexes. Geology, 34(11), 929-932.

640 Cortés, J. A., Smith, E. I., Valentine, G. A., Johnsen, R., Rasoazanamparany, C., Widom, E., ...
641 & Ruth, D. (2015). Intrinsic conditions of magma genesis at the Lunar Crater
642 Volcanic Field (Nevada), and implications for internal plumbing and magma ascent.
643 American Mineralogist, 100(2-3), 396-413
644 Duffield, W. A., Bacon, C. R., & Delaney, P. T. (1986). Deformation of poorly consolidated
645 sediment during shallow emplacement of a basalt sill, Coso Range, California. Bulletin
646 of volcanology, 48(2-3), 97-107.
647 Doré, A. G., & Lundin, E. R. (1996). Cenozoic compressional structures on the NE Atlantic
648 margin; nature, origin and potential significance for hydrocarbon exploration.
649 Petroleum Geoscience, 2(4), 299-311.
650 Doré, A. G., Lundin, E. R., Birkeland, O., Eliassen, P. E., & Jensen, L. N. (1997). The NE
651 Atlantic margin; implications of late Mesozoic and Cenozoic events for hydrocarbon
652 prospectivity. Petroleum Geoscience, 3(2), 117-131.
653 Ebdon, C. C., Granger, P. J., Johnson, H. D., & Evans, A. M. (1995). Early Tertiary evolution
654 and sequence stratigraphy of the Faeroe-Shetland Basin: implications for
655 hydrocarbon prospectivity. Geological Society, London, Special Publications, 90(1),
656 51-69.
657 Eide, C. H., Schofield, N., Jerram, D. A., & Howell, J. A. (2016). Basin-scale architecture of
658 deeply emplaced sill complexes: Jameson Land, East Greenland. Journal of the
659 Geological Society, 18.
660 Ellis, D., & Stoker, M. S. (2014). The Faroe–Shetland Basin: A regional perspective from the
661 Paleocene to the present day and its relationship to the opening of the North
662 Atlantic Ocean. Geological Society, London, Special Publications, 397(1), 11-31.

663 Fitch, F.J., Heard, G.L. & Miller, J.A. (1988) Basaltic magmatism of late Cretaceous and
664 Palaeogene age recorded in wells NNE of the Shetlands. Geol. Soc. Lond. Spec. Publ.,
665 39, 253–262.
666 Gaffney, E. S., Damjanac, B., & Valentine, G. A. (2007). Localization of volcanic activity: 2.
667 Effects of pre-existing structure. Earth and Planetary Science Letters, 263(3), 323-338.
668 Galland, O., Gisler, G. R., & Haug, Ø. T. (2014). Morphology and dynamics of explosive
669 vents through cohesive rock formations. Journal of Geophysical Research: Solid
670 Earth, 119(6), 4708-4728.
671 Grove, C. (2013) Submarine hydrothermal vent complexes in the Paleocene of the Faroe-
672 Shetland Basin: insights from three dimensional seismic and petrographical data.
673 Geology, 41, 71–74.
674 Gudmundsson, A., & Brenner, S. L. (2004). How mechanical layering affects local stresses,
675 unrests, and eruptions of volcanoes. Geophysical Research Letters, 31(16).
676 Gudmundsson, A. (2011). Deflection of dykes into sills at discontinuities and magma-
677 chamber formation. Tectonophysics, 500(1), 50-64.
678 Hansen, D. M. (2006). The morphology of intrusion-related vent structures and their
679 implications for constraining the timing of intrusive events along the NE Atlantic
680 margin. Journal of the Geological Society, 163(5), 789-800.
681 Hansen, D. M., & Cartwright, J. (2006). The three-dimensional geometry and growth of
682 forced folds above saucer-shaped igneous sills. Journal of Structural Geology, 28(8),
683 1520-1535.
684 Hernando, I. R., Franzese, J. R., Llambías, E. J., & Petrinovic, I. A. (2014). Vent distribution in
685 the Quaternary Payún Matrú Volcanic Field, western Argentina: Its relation to
686 tectonics and crustal structures. Tectonophysics, 622, 122-134.

687 Hitchen, K., & Ritchie, J. D. (1987). Geological review of the West Shetland area. Petroleum
688 Geology of North West Europe. Graham & Trotman, London, 737-749.
689 Holford, S. P., Tassone, D. R., Stoker, M. S., & Hillis, R. R. (2016). Contemporary stress
690 orientations in the Faroe–Shetland region. Journal of the Geological Society, 173(1),
691 142-152.
692 Jackson, M. D., & Pollard, D. D. (1988). The laccolith-stock controversy: New results from
693 the southern Henry Mountains, Utah. Geological Society of America Bulletin, 100(1),
694 117-139.
695 Jackson, C. A. L. (2012). Seismic reflection imaging and controls on the preservation of
696 ancient sill-fed magmatic vents. Journal of the Geological Society, 169(5), 503-506.
697 Jackson, C. A., Schofield, N., & Golenkov, B. (2013). Geometry and controls on the
698 development of igneous sill–related forced folds: A 2-D seismic reflection case study
699 from offshore southern Australia. Geological Society of America Bulletin, 125(11-12),
700 1874-1890.
701 Jamtveit, B., Svensen, H., Podladchikov, Y. Y., & Planke, S. (2004). Hydrothermal vent
702 complexes associated with sill intrusions in sedimentary basins. Physical geology of
703 high-level magmatic systems, 234, 233-241.
704 Johnson, E. R., Wallace, P. J., Cashman, K. V., Granados, H. D., & Kent, A. J. (2008).
705 Magmatic volatile contents and degassing-induced crystallization at Volcán Jorullo,
706 Mexico: implications for melt evolution and the plumbing systems of monogenetic
707 volcanoes. Earth and Planetary Science Letters, 269(3), 478-487.
708 Jolly, R. J. H., & Sanderson, D. J. (1997). A Mohr circle construction for the opening of a pre-
709 existing fracture. Journal of Structural Geology, 19(6), 887-892.

710 Kavanagh, J. L., Menand, T., & Sparks, R. S. J. (2006). An experimental investigation of sill
711 formation and propagation in layered elastic media. Earth and Planetary Science
712 Letters, 245(3), 799-813.
713 Kavanagh, J. L., Boutelier, D., & Cruden, A. R. (2015). The mechanics of sill inception,
714 propagation and growth: Experimental evidence for rapid reduction in magmatic
715 overpressure. Earth and Planetary Science Letters, 421, 117-128.
716 Kereszturi, G., & Németh, K. (2012). Monogenetic basaltic volcanoes: genetic classification,
717 growth, geomorphology and degradation. INTECH Open Access Publisher.
718 Kiyosugi, K., Connor, C. B., Wetmore, P. H., Ferwerda, B. P., Germa, A. M., Connor, L. J., &
719 Hintz, A. R. (2012). Relationship between dike and volcanic conduit distribution in a
720 highly eroded monogenetic volcanic field: San Rafael, Utah, USA. Geology, 40(8),
721 695-698.
722 Kokelaar, B. P. (1983). The mechanism of Surtseyan volcanism. Journal of the Geological
723 Society, 140(6), 939-944.
724 Kokelaar, P. (1986). Magma-water interactions in subaqueous and emergent basaltic. Bulletin
725 of Volcanology, 48(5), 275-289.
726 Knott, S. D.,Burchell, M. T., Jolley, E. J., and Fraser, A. J. (1993) Mesozoic and Cenozoic plate
727 reconstruction of the North Atlantic and hydrocarbon plays of the Atlantic margins
728 *in* Petroleum geology of northwest Europe, proceedings of the 4th conference. Ed.
729 Parker, J R. London, The Geological Society
730 Lamers, E., & Carmichael, S. M. M. (1999, January). The Paleocene deepwater sandstone play
731 West of Shetland. In Geological Society, London, Petroleum Geology Conference
732 series (Vol. 5, pp. 645-659). Geological Society of London.

733 Le Corvec, N., Spörli, K. B., Rowland, J., & Lindsay, J. (2013). Spatial distribution and
734 alignments of volcanic centers: clues to the formation of monogenetic volcanic fields.
735 Earth-Science Reviews, 124, 96-114.
736 Lefebvre, N. S., White, J. D. L., & Kjarsgaard, B. A. (2012). Spatter-dike reveals subterranean
737 magma diversions: Consequences for small multivent basaltic eruptions. Geology,
738 40(5), 423-426.
739 Magee, C., Jackson, C. A. L., & Schofield, N. (2013). The influence of normal fault geometry
740 on igneous sill emplacement and morphology. Geology, 41(4), 407-410.
741 Magee, C., Jackson, C. L., & Schofield, N. (2014). Diachronous sub‐volcanic intrusion along
742 deep‐water margins: insights from the Irish Rockall Basin. Basin Research, 26(1),
743 85-105.
744 Magee, C., Muirhead, J. D., *et al.* (2016). Lateral magma flow in mafic sill complexes.
745 Geosphere, GES01256-1.
746 Manton, B. (2015) The mechanics of sill propagation and associated venting, investigated
747 using 3D seismic data from offshore Norway. PhD Thesis, Cardiff University.
748 Mazzarini, F., Le Corvec, N., Isola, I., & Favalli, M. (2016). Volcanic field elongation, vent
749 distribution, and tectonic evolution of a continental rift: The Main Ethiopian Rift
750 example. Geosphere, 12(3), 706-720.
751 McArdle, N. J., & Ackers, M. A. (2012). Understanding seismic thin-bed responses using
752 frequency decomposition and RGB blending. First Break, 30(12).
753 McBirney, A. R., Taylor, H. P., & Armstrong, R. L. (1987). Paricutin re-examined: a classic
754 example of crustal assimilation in calc-alkaline magma. Contributions to Mineralogy
755 and Petrology, 95(1), 4-20.

Menand, T. (2008). The mechanics and dynamics of sills in layered elastic rocks and their implications for the growth of laccoliths and other igneous complexes. Earth and Planetary Science Letters, 267(1), 93-99.

Millett, J. M., Hole, M. J., Jolley, D. W., Schofield, N., & Campbell, E. (2016). Frontier exploration and the North Atlantic Igneous Province: new insights from a 2.6 km offshore volcanic sequence in the NE Faroe–Shetland Basin. Journal of the Geological Society, 173(2), 320-336.

Moy, D. J., & Imber, J. (2009). A critical analysis of the structure and tectonic significance of rift-oblique lineaments ('transfer zones') in the Mesozoic–Cenozoic succession of the Faroe–Shetland Basin, NE Atlantic margin. Journal of the Geological Society, 166(5), 831-844.

Muirhead, J. D., Airoldi, G., Rowland, J. V., & White, J. D. (2012). Interconnected sills and inclined sheet intrusions control shallow magma transport in the Ferrar large igneous province, Antarctica. Geological Society of America Bulletin, 124(1-2), 162-180.

Muirhead, J. D., Kattenhorn, S. A., & Le Corvec, N. (2015). Varying styles of magmatic strain accommodation across the East African Rift. Geochemistry, Geophysics, Geosystems, 16(8), 2775-2795.

Muirhead, J. D., Van Eaton, A. R., Re, G., White, J. D., & Ort, M. H. (2016). Monogenetic volcanoes fed by interconnected dikes and sills in the Hopi Buttes volcanic field, Navajo Nation, USA. Bulletin of Volcanology, 78(2), 1-16.

Muirhead, J. D., Kattenhorn, S. A., Lee, H., Mana, S., Turrin, B. D., Fischer, T. P., Kianji, G., Dindi, E., and Stamps D. S (2016b). Evolution of upper crustal faulting assisted by magmatic volatile release during early-stage continental rift development in the East African Rift. Geosphere, GES01375-1.

780 Naylor, P. H., Bell, B. R., Jolley, D. W., Durnall, P., & Fredsted, R. (1999, January).
781 Palaeogene magmatism in the Faeroe–Shetland Basin: influences on uplift history and
782 sedimentation. In Geological Society, London, Petroleum Geology Conference series
783 (Vol. 5, pp. 545-558). Geological Society of London.
784 Németh, K. (2010). Monogenetic volcanic fields: origin, sedimentary record, and relationship
785 with polygenetic volcanism. Geological Society of America Special Papers, 470, 43-66.
786 Németh, K., White, J. D., Reay, A., & Martin, U. (2003). Compositional variation during
787 monogenetic volcano growth and its implications for magma supply to continental
788 volcanic fields. Journal of the Geological Society, 160(4), 523-530.
789 Németh, K., & Martin, U. (2007). Shallow sill and dyke complex in western Hungary as a
790 possible feeding system of phreatomagmatic volcanoes in "soft-rock" environment.
791 Journal of Volcanology and Geothermal Research, 159(1), 138-152
792 Neidell, N. S. (1979). Stratigraphic modeling and interpretation: Geophysical principles and
793 techniques (No. 13). American Association of Petroleum Geologists.
794 Passey, S. R., & Jolley, D. W. (2008). A revised lithostratigraphic nomenclature for the
795 Palaeogene Faroe Islands Basalt group, NE Atlantic Ocean. Earth and Environmental
796 Science Transactions of the Royal Society of Edinburgh, 99(3-4), 127-158.
797 Passey, S., Hitchen, K., (2011) Cenozoic (igneous) *in* Ritchie, J. D., Ziska, H., Johnson, H., &
798 Evans, D. Eds. Geology of the Faroe-Shetland Basin and adjacent areas. British
799 Geological Survey, Nottingham, UK.
800 Paulsen, T. S., & Wilson, T. J. (2010). New criteria for systematic mapping and reliability
801 assessment of monogenetic volcanic vent alignments and elongate volcanic vents for
802 crustal stress analyses. Tectonophysics, 482(1), 16-28.
803 Planke, S., Rasmussen, T., Rey, S. S., & Myklebust, R. (2005). Seismic characteristics and
804 distribution of volcanic intrusions and hydrothermal vent complexes in the Vøring

805 and Møre basins. In Geological Society, London, Petroleum Geology Conference
806 series (Vol. 6, pp. 833-844). Geological Society of London.
807 Pollard, D. D., Muller, O. H., & Dockstader, D. R. (1975). The form and growth of fingered
808 sheet intrusions. Geological Society of America Bulletin, 86(3), 351-363.
809 Polteau, S., Mazzini, A., Galland, O., Planke, S., & Malthe-Sørenssen, A. (2008). Saucer-
810 shaped intrusions: occurrences, emplacement and implications. Earth and Planetary
811 Science Letters, 266(1), 195-204
812 Re, G., White, J. D. L., & Ort, M. H. (2015). Dikes, sills, and stress-regime evolution during
813 emplacement of the Jagged Rocks Complex, Hopi Buttes Volcanic Field, Navajo
814 Nation, USA. Journal of Volcanology and Geothermal Research, 295, 65-79.
815 Re, G., White, J. D., Muirhead, J. D., & Ort, M. H. (2016). Subterranean fragmentation of
816 magma during conduit initiation and evolution in the shallow plumbing system of the
817 small-volume Jagged Rocks volcanoes (Hopi Buttes Volcanic Field, Arizona, USA).
818 Bulletin of Volcanology, 78(8), 55.
819 Richardson, J. A., Connor, C. B., Wetmore, P. H., Connor, L. J., & Gallant, E. A. (2015). Role
820 of sills in the development of volcanic fields: Insights from lidar mapping surveys of
821 the San Rafael Swell, Utah. Geology, 43(11), 1023-1026.
822 Ritchie, J. D., Gatliff, R. W., & Richards, P. C. (1999). Early Tertiary magmatism in the
823 offshore NW UK margin and surrounds. In Geological Society, London, Petroleum
824 Geology Conference series (Vol. 5, pp. 573-584). Geological Society of London.
825 Ritchie, J. D., Johnson, H., & Kimbell, G. S. (2003). The nature and age of Cenozoic
826 contractional deformation within the NE Faroe–Shetland Basin. Marine and
827 Petroleum Geology, 20(5), 399-409.
828 Ritchie, J. D., Ziska, H., Johnson, H., & Evans, D. Eds. (2011) Geology of the Faroe-Shetland
829 Basin and adjacent areas. British Geological Survey, Nottingham, UK.

830 Rohrman, M. (2007). Prospectivity of volcanic basins: Trap delineation and acreage de-risking.
831 AAPG bulletin, 91(6), 915-939.
832 Rumph, B., Reaves, C.M., Orange, V.G. & Robinson, D.L. (1993) Structuring and Transfer
833 Zones in the Faroe Shetland Basin in a Regional Tectonic Context, 999–1009 in
834 Petroleum Geology of Northwest Europe, Proceedings of the 4th Conference (Ed.
835 by J.R. Paerker). The Geological Society, London.
836 Schofield, N., Stevenson, C., & Reston, T. (2010). Magma fingers and host rock fluidization in
837 the emplacement of sills. Geology, 38(1), 63-66.
838 Schofield, N. J., Brown, D. J., Magee, C., & Stevenson, C. T. (2012). Sill morphology and
839 comparison of brittle and non-brittle emplacement mechanisms. Journal of the
840 Geological Society, 169(2), 127-141.
841 Schofield, N., & Jolley, D. W. (2013). Development of intra-basaltic lava-field drainage
842 systems within the Faroe–Shetland Basin. Petroleum Geoscience, 19(3), 273-288.
843 Schofield, N., Alsop, I., Warren, J., Underhill, J. R., Lehné, R., Beer, W., & Lukas, V. (2014).
844 Mobilizing salt: Magma-salt interactions. Geology, 42(7), 599-602.
845 Schofield, N., Holford, S., *et al. (*2015). Regional magma plumbing and emplacement
846 mechanisms of the Faroe‐Shetland Sill Complex: implications for magma transport
847 and petroleum systems within sedimentary basins. Basin Research
848 Smallwood, J. R., Staples, R. K., Richardson, K. R., & White, R. S. (1999). Crust generated
849 above the Iceland mantle plume: from continental rift to oceanic spreading center.
850 Journal of Geophysical Research: Solid Earth, 104, 22885-22902.
851 Smallwood, J. R., & Maresh, J. (2002). The properties, morphology and distribution of
852 igneous sills: modelling, borehole data and 3D seismic from the Faroe-Shetland area.
853 Geological Society, London, Special Publications, 197(1), 271-306.

854 Smallwood J. R., White R. S. (2002). Ridge-plume interaction in the North Atlantic and its
855 influence on continental breakup and seafloor spreading. In: Jolley D. W., Bell B. R.
856 (eds) The North Atlantic Igneous Province: Stratigraphy, Tectonic, Volcanic and
857 Magmatic Processes. Geological Society, London, Special Publications, 197, 15–37.
858 Smith, I. E. M., Blake, S., Wilson, C. J. N., & Houghton, B. F. (2008). Deep-seated
859 fractionation during the rise of a small-volume basalt magma batch: Crater Hill,
860 Auckland, New Zealand. Contributions to Mineralogy and Petrology, 155(4), 511-
861 527.
862 Smythe, D. K. (1983). Faeroe-Shetland escarpment and continental margin north of the
863 Faeroes. In Structure and Development of the Greenland-Scotland Ridge (pp. 109-
864 119). Springer US.
865 Svensen, H., Jamtveit, B., Planke, S., & Chevallier, L. (2006). Structure and evolution of
866 hydrothermal vent complexes in the Karoo Basin, South Africa. Journal of the
867 Geological Society, 163(4), 671-682.
868 Thomson, K., & Hutton, D. (2004). Geometry and growth of sill complexes: insights using
869 3D seismic from the North Rockall Trough. Bulletin of Volcanology, 66(4), 364-375.
870 Thomson, K. (2007). Determining magma flow in sills, dykes and laccoliths and their
871 implications for sill emplacement mechanisms. Bulletin of Volcanology, 70(2), 183-
872 201.
873 Thomson, K., & Schofield, N. (2008). Lithological and structural controls on the
874 emplacement and morphology of sills in sedimentary basins. Geological Society,
875 London, Special Publications, 302(1), 31-44.
876 Tibaldi, A. (2015). Structure of volcano plumbing systems: A review of multi-parametric
877 effects. Journal of Volcanology and Geothermal Research, 298, 85-135.

878 Valentine, G. A., & Krogh, K. E. (2006). Emplacement of shallow dikes and sills beneath a
879 small basaltic volcanic center–The role of pre-existing structure (Paiute Ridge,
880 southern Nevada, USA). Earth and Planetary Science Letters, 246(3), 217-230.
881 Valentine, G. A., & Perry, F. V. (2007). Tectonically controlled, time-predictable basaltic
882 volcanism from a lithospheric mantle source (central Basin and Range Province,
883 USA). Earth and Planetary Science Letters, 261(1), 201-216.
884 Waagstein, R. (1988). Structure, composition and age of the Faeroe basalt plateau.
885 Geological Society, London, Special Publications, 39(1), 225-238.
886 White, R. S. (1989) Initiation of the Iceland Plume and Opening of the North Atlantic:
887 Chapter 10: North Atlantic Perspectives. 149-154.
888 White, J. D., & Ross, P. S. (2011). Maar-diatreme volcanoes: a review. Journal of Volcanology
889 and Geothermal Research, 201(1), 1-29.
890 Wood, C. A. (1980). Morphometric evolution of cinder cones. Journal of Volcanology and
891 Geothermal Research, 7(3), 387-413.
892 Wright, K. A., Davies, R. J., Jerram, D. A., Morris, J., & Fletcher, R. (2012). Application of
893 seismic and sequence stratigraphic concepts to a lava‐fed delta system in the
894 Faroe‐Shetland Basin, UK and Faroes. Basin Research, 24(1), 91-106.
895 Wright, K. A. (2013) Seismic Stratigraphy and Geomorphology of Palaeocene Volcanic
896 Rocks, Faroe-Shetland Basin. Doctoral thesis, Durham University.

897 **Figure Captions**

898 **Fig. 1**: (A) Structural map of the Faroe-Shetland Basin and NE Rockall, highlighting the NE-
899 SW trending sub-basins and NW-SE trending lineaments. Faroe-Shetland Escarpment
900 marked by dashed line (from Ritchie *et al.* 2011 and Archer *et al.* 2005). Location of the
901 Rockall Dome (Dome 164/7-1) marked by dotted line. Cross-section B-B' shown in Fig. 3.

902 Inset shown in (B). (B) Location of 3D seismic dataset (dashed line) and distribution of wells
903 are marked. Cross-sections A-A' in Fig. 2 and C-C' in Fig. 5 (solid black line). (C) Gravity
904 data over the Brendan's Volcanic Centre (BVC). Green shading shows high (positive) gravity
905 response; blue shows low (negative) gravity response. Locations of gravity anomalies
906 highlighted by red solid lines. Bouguer anomaly across the BVC is +80mGal. White dotted
907 lines highlight the proposed structural highs including the BNS. Black solid line shows
908 location of (B).
909
910 **Fig. 2**: **(A)** Representative seismic line and interpreted line of the Ben Nevis Structure
911 (BNS) (A-A') displaying location of well 219/21-1. Note the variation in thickness of the
912 Upper Cretaceous on either side of the BNS and the truncation of bright reflectors on the
913 flank of the NW BNS. Location of cross-section shown in Fig.1B. **(B)** Chronostratigraphic
914 log of well 219/21-1. Sills in Kyrre Formation dated by Rohrman (2007). **(C)** 3D structural
915 map of the BNS showing 4-way dip structure.
916
917 **Fig. 3**: Interpreted regional seismic line across between the Ben Nevis Structure (BNS) and
918 Lagavulin prospects (Data courtesy of PGS CRRG 2D GeoStreamer®). The location of the
919 cross-section shown in Fig. 1A (B-B'). "B" is on the left and "B"' is on the right of the
920 seismic line. Well sites labelled. Interpreted stratigraphy shows the western margin of the
921 BNS is onlapped by T38-T31 sediments and T40 volcanic rocks extrapolated from the
922 Lagavulin well shown in Fig. 1A. The lava sequence in the Ben Nevis seismic dataset (Fig. 2)
923 is an earlier and localised T36 lava field (blue). T-sequence stratigraphy in Fig. 4.
924
925 **Fig. 4**: Palaeogene stratigraphy of the Faroe-Shetland Basin (FSB) (adapted from Schofield &
926 Jolley 2013), with BGS lithostratigraphy (Ritchie *et al.* 2011); BP T-sequence stratigraphy

927 (after Ebdon *et al*. 1995), and the North Sea equivalent Hordaland Group lithostratigraphy
928 (found in wells east of the BNS).
929
930 **Fig. 5**: Truncation of sills along the Upper Cretaceous unconformity (green arrows) and
931 subsequent onlapping of Upper Palaeocene stratigraphy. Location of Fig. 5 shown in Fig. 2.
932 Location of seismic line in inset.
933
934 **Fig. 6**: **(A)** Seismic line and interpreted line (C-C' in Fig. 1B) showing the relationship
935 between the BNS and the underlying sill complex. Magma migrates from the Faroe-Shetland
936 Sill Complex (FSSC) towards the palaeo-high (BNS), where it encounters the inclined flank
937 of the BNS, allowing magma to migrate towards the surface. Lateral magma migration is up
938 to 10 km. The Faroe-Shetland Escarpment (FSE) is clearly distinguished, marked by a change
939 in seismic responses from high amplitude, continuous reflectors to chaotic package of
940 discontinuous bright reflectors over the scarp, representative of lavas feeding hyaloclastite
941 foresets. **(B)** Top volcanic surface with the FSE indicated. Mounds in the Erlend Sub-basin
942 highlighted as a series of forced folds, caused by the emplacement of shallow intrusions.
943
944 **Fig. 7**: Seismic cross-sections with interpretations through some of the monogenetic
945 edifices showing an affinity between the volcanic cone on the top volcanic surface and an
946 underlying sill. Solid yellow lines highlight prominent interpreted lava flows, dashed blue lines
947 indicate (approximately) the base of the volcanic sequence and solid green lines highlight
948 intrusions. Time slices of each edifice show an organised internal structure. Edifice 9, the
949 submarine volcanic cone, appears to have a more disorganised structure. Spectral
950 decomposition of the top volcanic surface highlights the lava flows emanating from edifice 6
951 and 7. Map insets show location of each edifice.

952

953 **Fig. 8**: Comparison of sill morphologies. Bright reflectors indicate intrusions. **(A)** saucer-
954 shaped; **(B)** climbing saucer-shaped; and **(C)** planar transgressive sheet (Planke *et al.* 2005).
955 **(D)** Distribution of sill morphologies, where transgressive sheets are located along the
956 flanks of the BNS, whereas saucer and climbing-saucer shaped sills are exclusively within the
957 Erlend Sub-basin. **(E)(F)** Opacity rendered images of transgressive sheets feeding edifices
958 on the top volcanic surface. Coalesced magma lobes are evident and are used as a magma
959 flow indicator. Map insets show direction of view.

960

961 **Fig. 9**: **(A)** Seismic line and interpreted line through a buried cone (A) beneath a later
962 edifice (B). Edifice A is onlapped by lavas and inter-lava sediments. A singular intrusion
963 appears to feed both edifice-forming events, however the high amplitude reflector likely
964 represents multiple, stacked intrusions. Sill A fed Edifice A and sill B fed Edifice B. Map inset
965 shows location of seismic line **(B)** Structural map of the top volcanic surface showing the
966 location of the Edifice B. Location of the buried cone, Edifice A, is highlighted by circle. The
967 structural map shows the lateral proximity of the cones to each other.

968

969 **Fig. 10**: Structural map of the top volcanic surface. Edifices are highlighted by solid white
970 lines and appear to be distributed around the axis of the BNS pericline (black dashed line).
971 On the NW side of the BNS axis, an ENE-WSW and NE-SW alignment is apparent. (B)
972 Outlines of the edifices were used to create a best-fit line and each spacing distance was
973 measured. Inset, the angle between the longest axis and the best-fit line was also measured.
974 Using the Paulsen & Wilson (2010) method for statistical alignment analysis, this alignment
975 was deemed statistically invalid, however an alignment is clearly evident.

976

977 **Fig. 11**: Illustrated reconstruction of the evolution of the BNS structure and subsequent
978 volcanic activity. Not to scale. Time 1: Emplacement of laccolith and associated intrusions
979 created uplift and updoming of the U. Cretaceous stratigraphy, creating a local palaeohigh
980 which was subsequently exposed to subaerial erosion. Time 2: Continued erosion of the
981 palaeohigh causing truncation of intrusions and creation of the U Cretaceous unconformity.
982 Upper Palaeocene stratigraphy deposited into sub-basin to the NE of the palaeohigh, likely
983 sourced from the erosion of the structure and from products and reworked products of the
984 Brendans Volcanic Centre (to the NE). Compaction of the U. Cretaceous stratigraphy
985 occurs only on the NE of the palaeohigh due to localised deposition of Palaeocene strata.
986 Time 3: Onset of main volcanic activity initiated by deposition of hyaloclastite packages, and
987 lava flows. The former palaeohigh (now fully eroded) is overstepped by subsequent lava
988 flows feeding hyaloclastite packages when they reach the FSE on the SE of the BNS.
989 Monogenetic volcanism occurs throughout main volcanic activity, producing isolated lavas.
990
991 **Fig. 12**: **(A)** Preferred interpretation for the uplift of the Ben Nevis Structure, involving the
992 emplacement of a laccolith and associated intrusions. Inflation and updoming of the laccolith
993 and intrusions cause localized uplift, and significant heating of the Upper Cretaceous
994 stratigraphy (adapted from Jackson & Pollard, 1988 and Archer *et al.* 2005). **(B)** Jackson and
995 Pollard (1988) three-stage model on the progression of laccolith emplacement and uplift at
996 the Henry Mountains, Colorado Plateau, USA.
997
998 **Fig. 13**: Schematic diagram illustrating the development of stacked intrusions (adapted from
999 Kavanagh *et al.* 2006). Sub-horizontal propagation occurs at a host-rock interface where
1000 there is a high rigidity contrast. Arrows show direction of magma migration. When the sill

freezes, it creates a rigidity contrast with the surrounding host-rock, generating a favourable environment for later magma emplacement.

Fig. 14: Mechanisms of transgressive sheet propagation. **(A)** Inclined rheological boundary with a sufficient rigidity contrast to rotate σ_1, allows propagation of magma along an inclined pathway. **(B)** The inflation of an intrusion causes forced fold formation in the overburden. Extensional fractures develop at the tip of the sill, instigating host-rock fluidisation around the sill tip. Magma exploits fluidised host-rock. Adapted from Schofield *et al.* (2010). **(C)** Application of load to the top surface (in this case, the development of a scoria cone), reorients the compressive stresses of the host-rock, promoting the migration of magma in an inclined sheet. Adapted from Re *et al.* (2015).

Figure 1

Click here to download Figure Figure 1.jpg

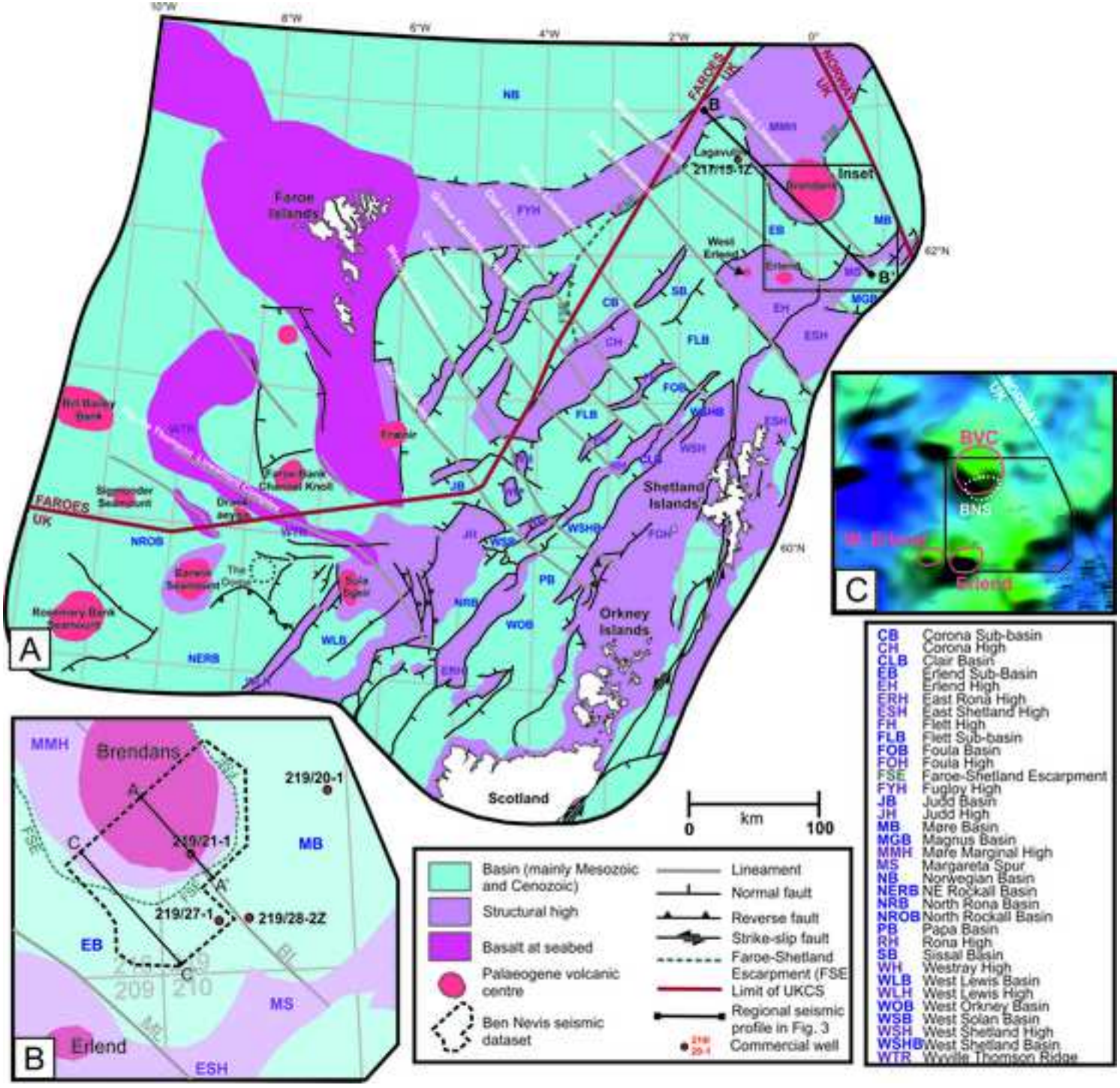

Figure 2

Click here to download Figure Figure 2.jpg

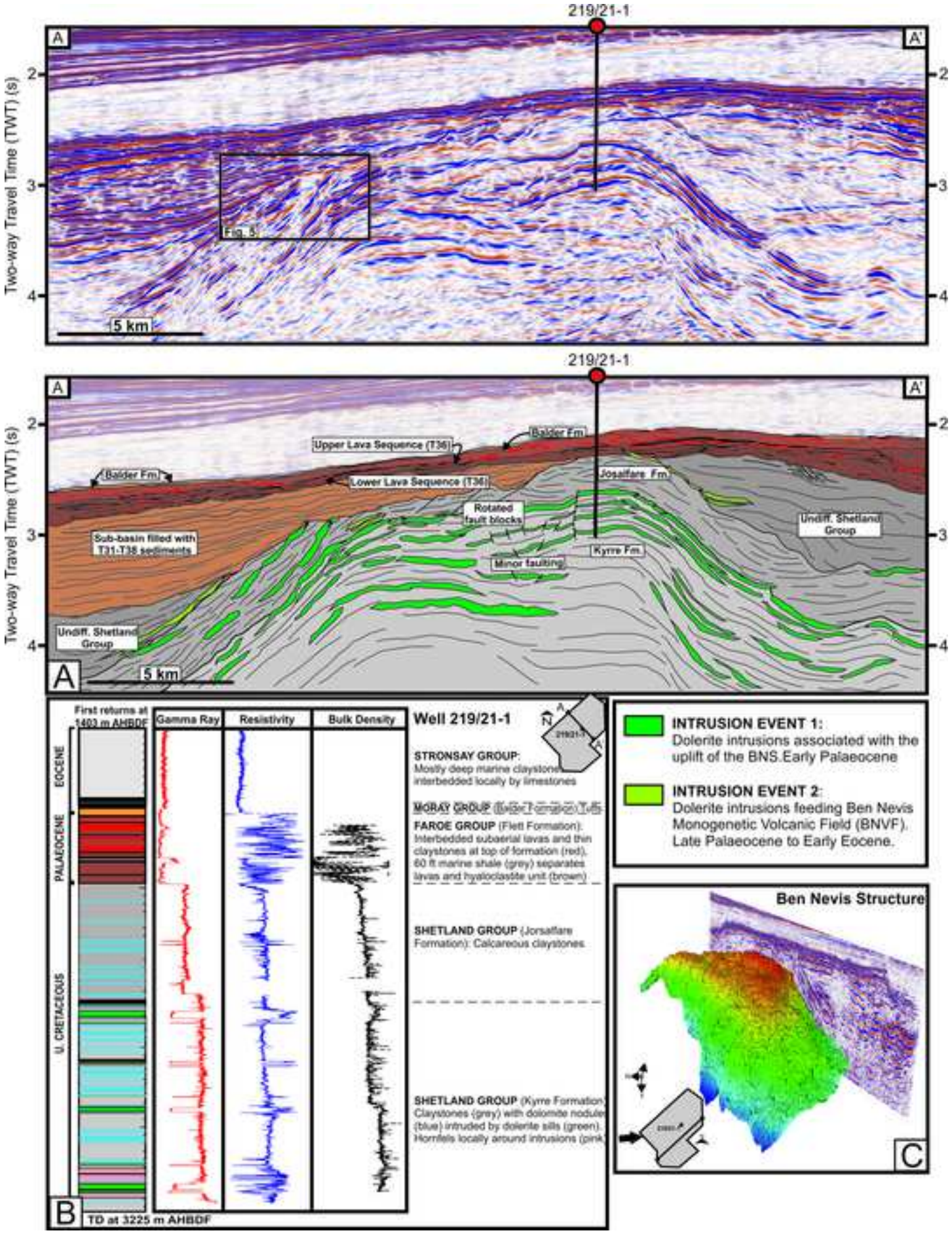

Figure 3

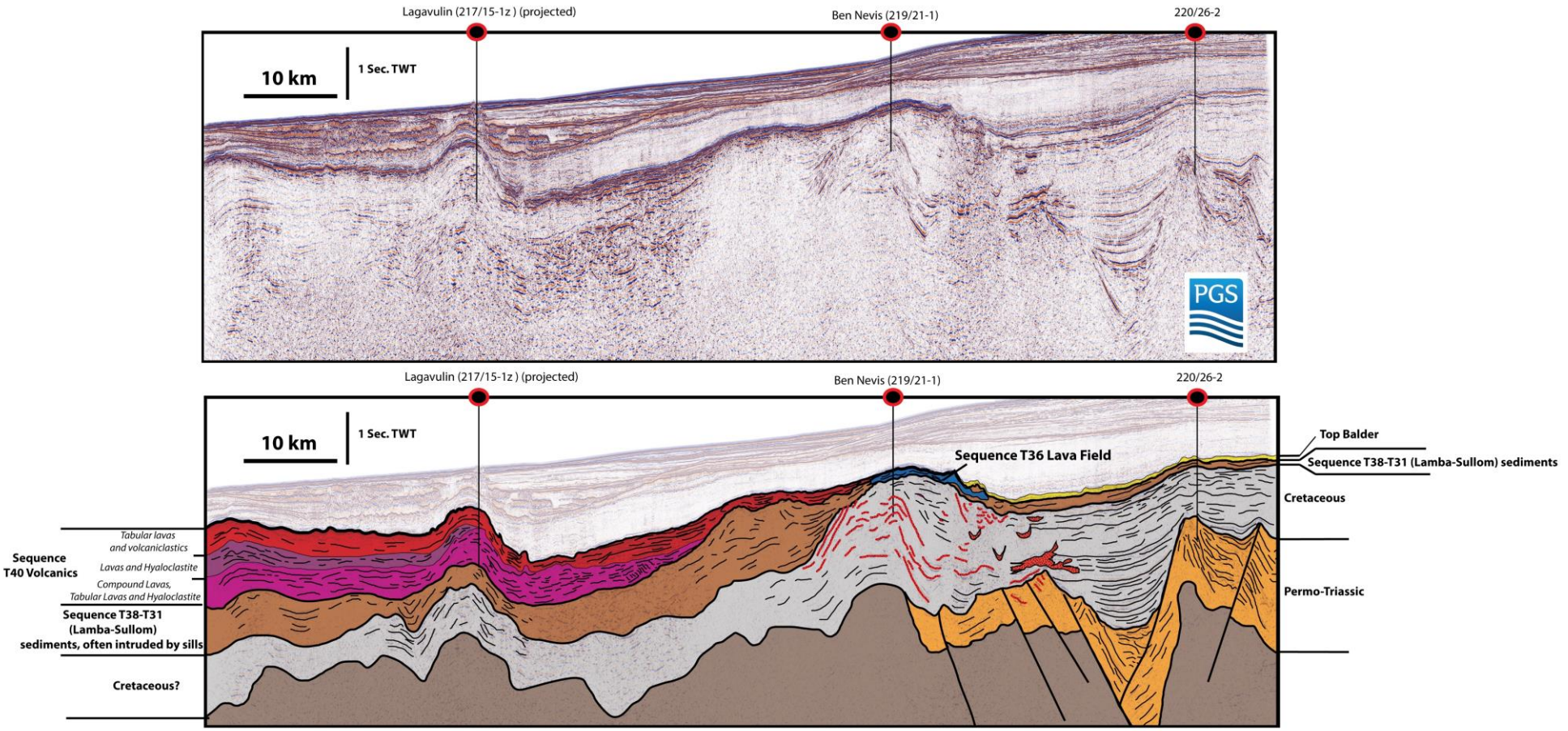

Figure 4

Click here to download Figure Figure 4.jpg

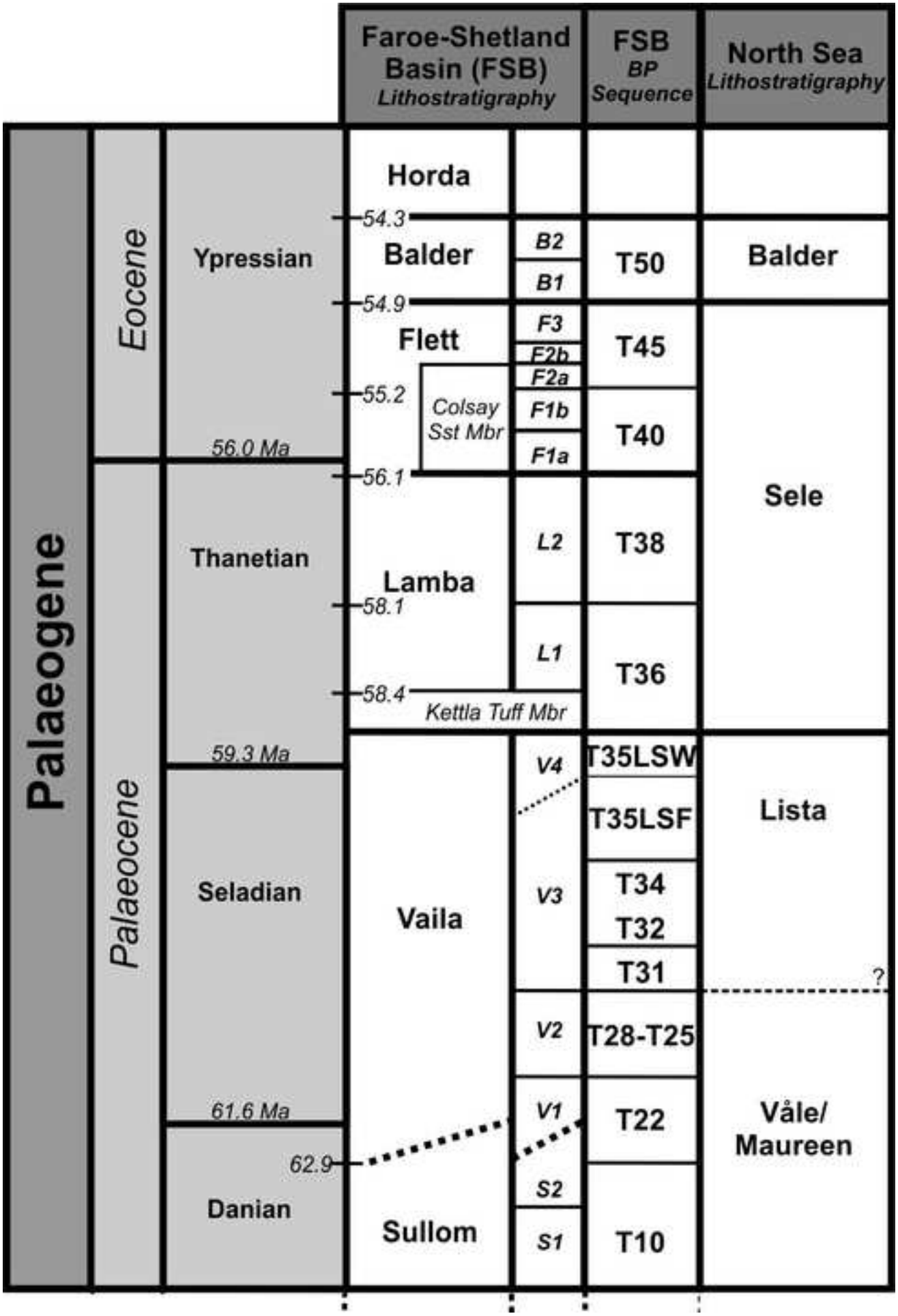

Figure 5

Click here to download Figure Figure 5.jpg

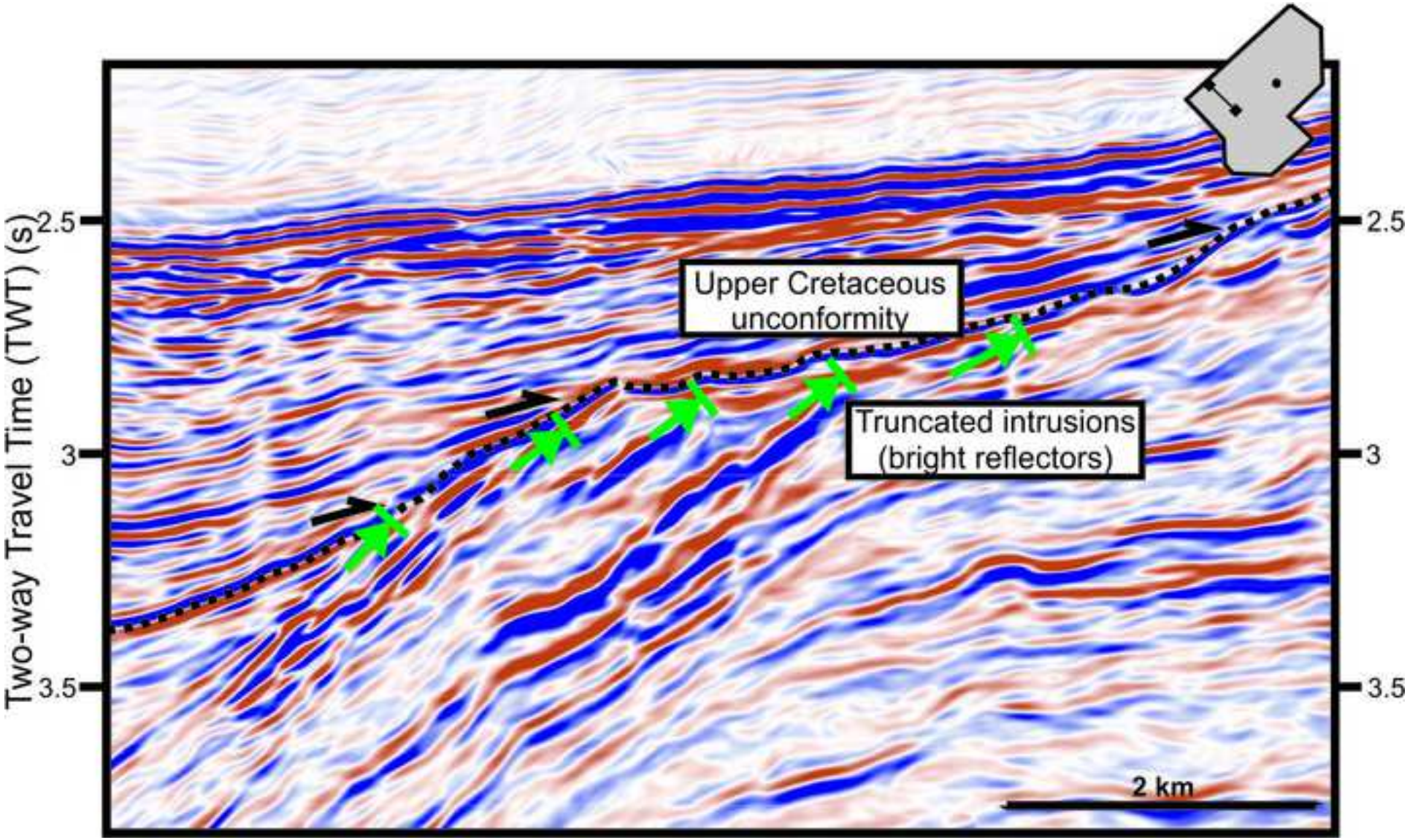

Figure 6

Click here to download Figure Figure 6 compressed.jpg

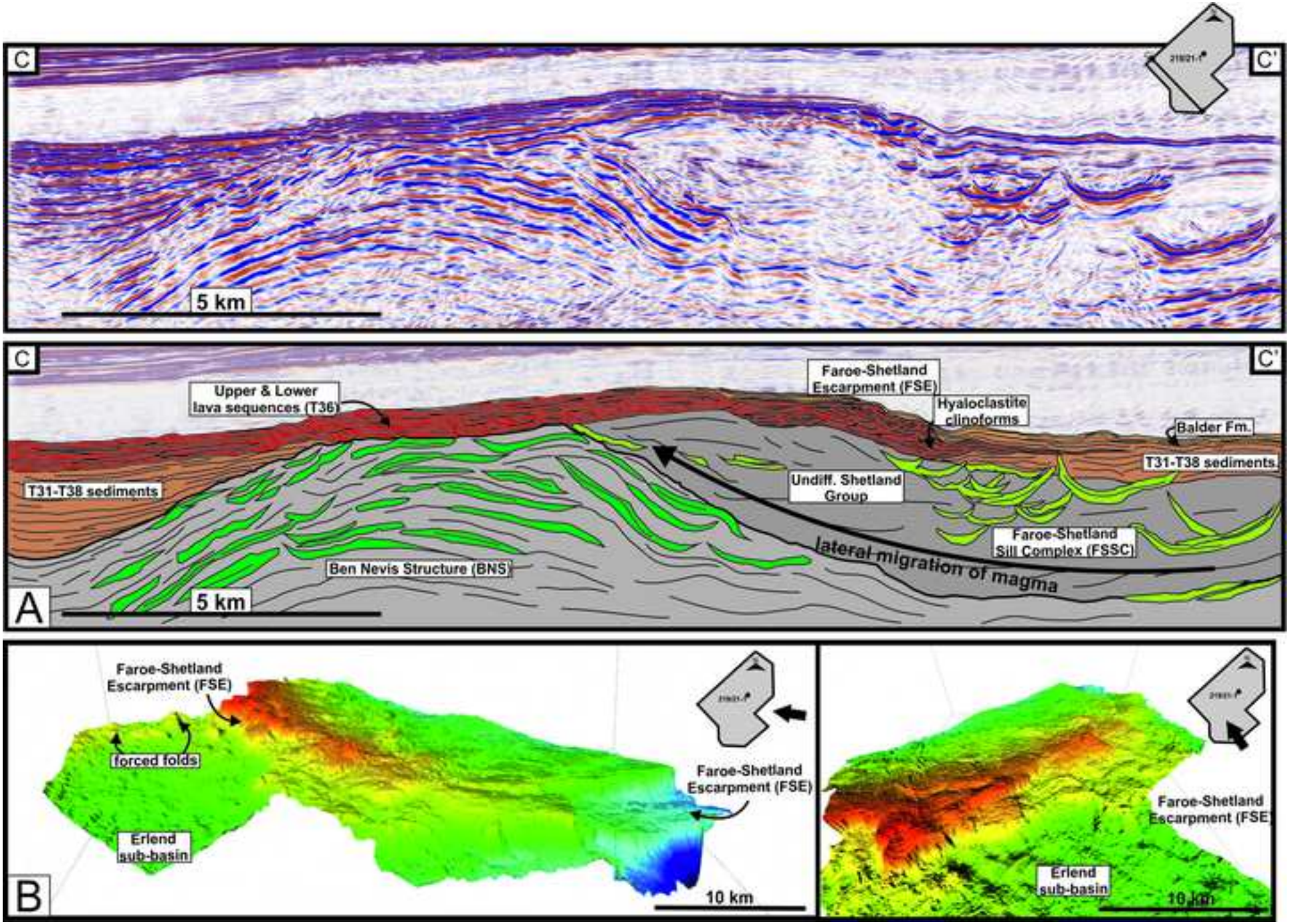

Figure 7

Click here to download Figure Figure 7.jpg

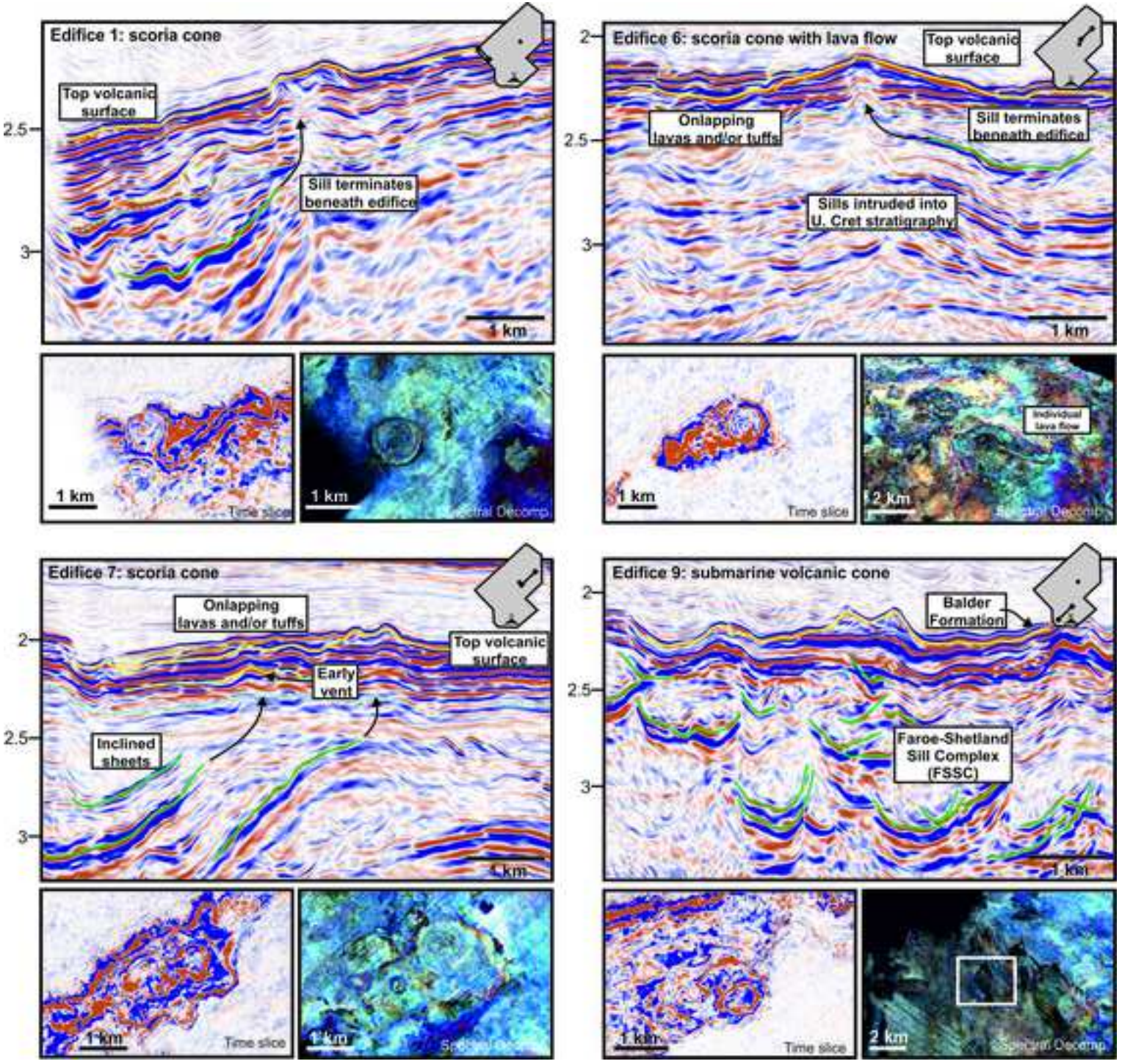

Figure 8

Click here to download Figure Figure 8.jpg

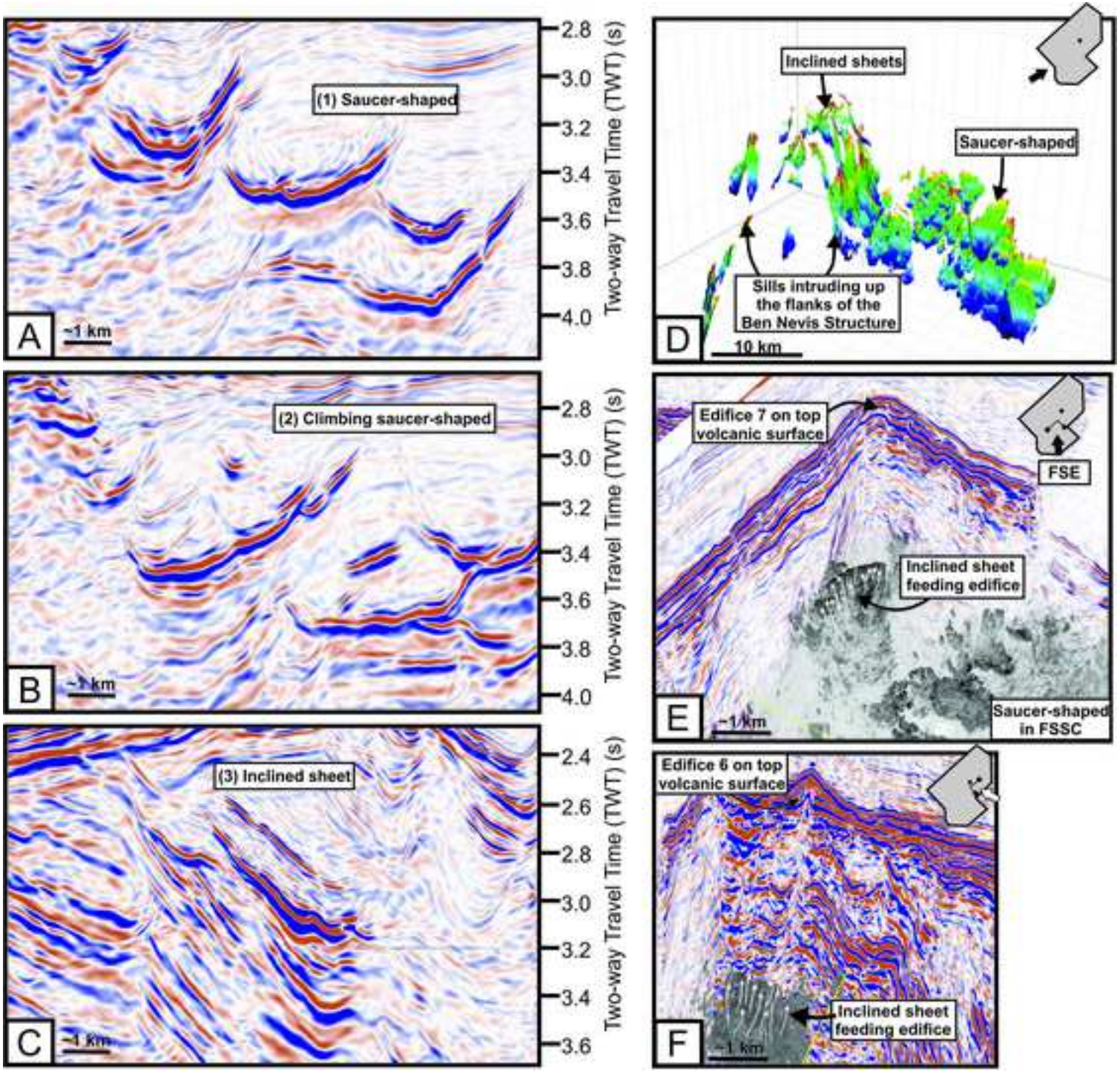

Figure 9

Click here to download Figure Figure 9.jpg

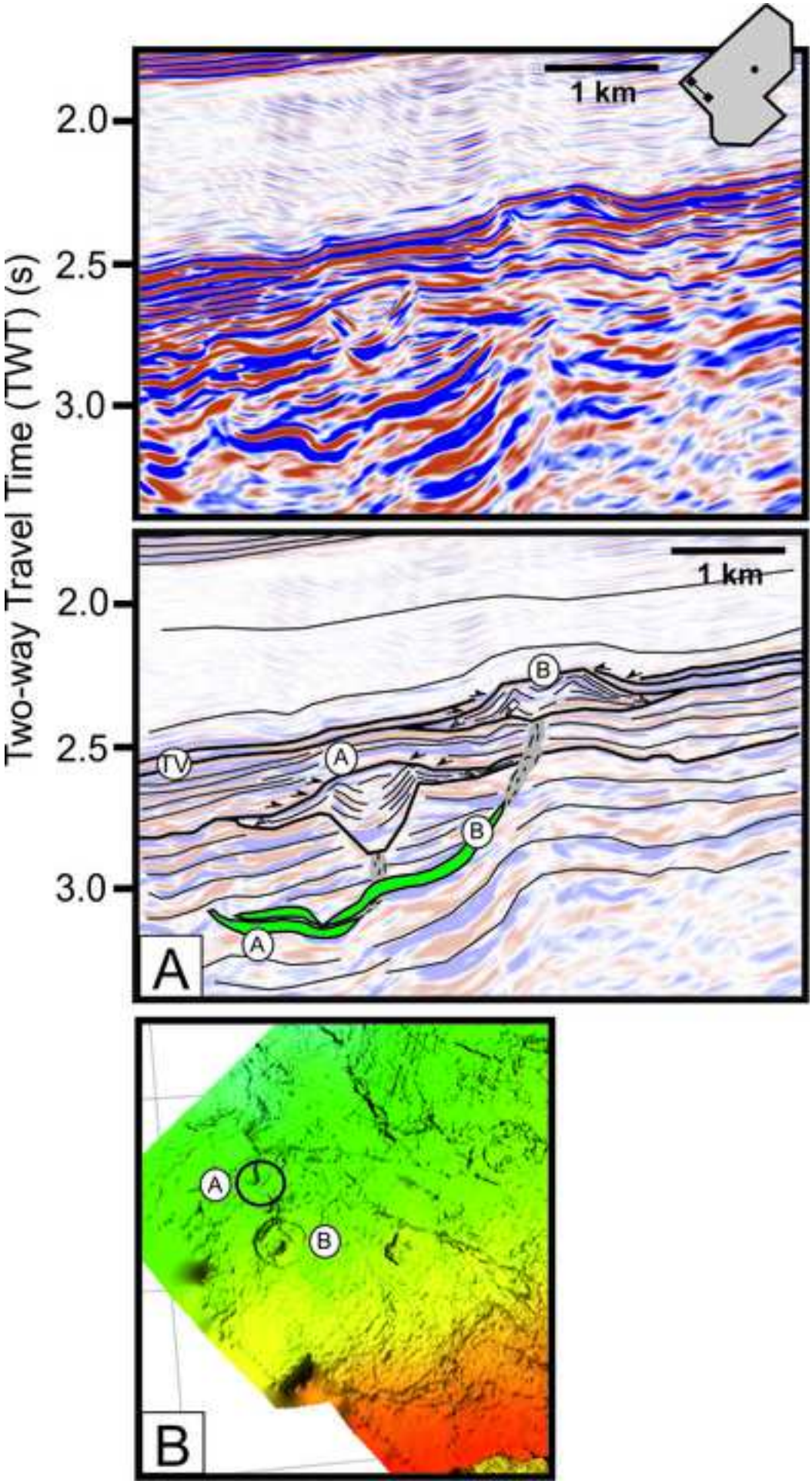

Figure 10

Click here to download Figure Figure 10..jpg

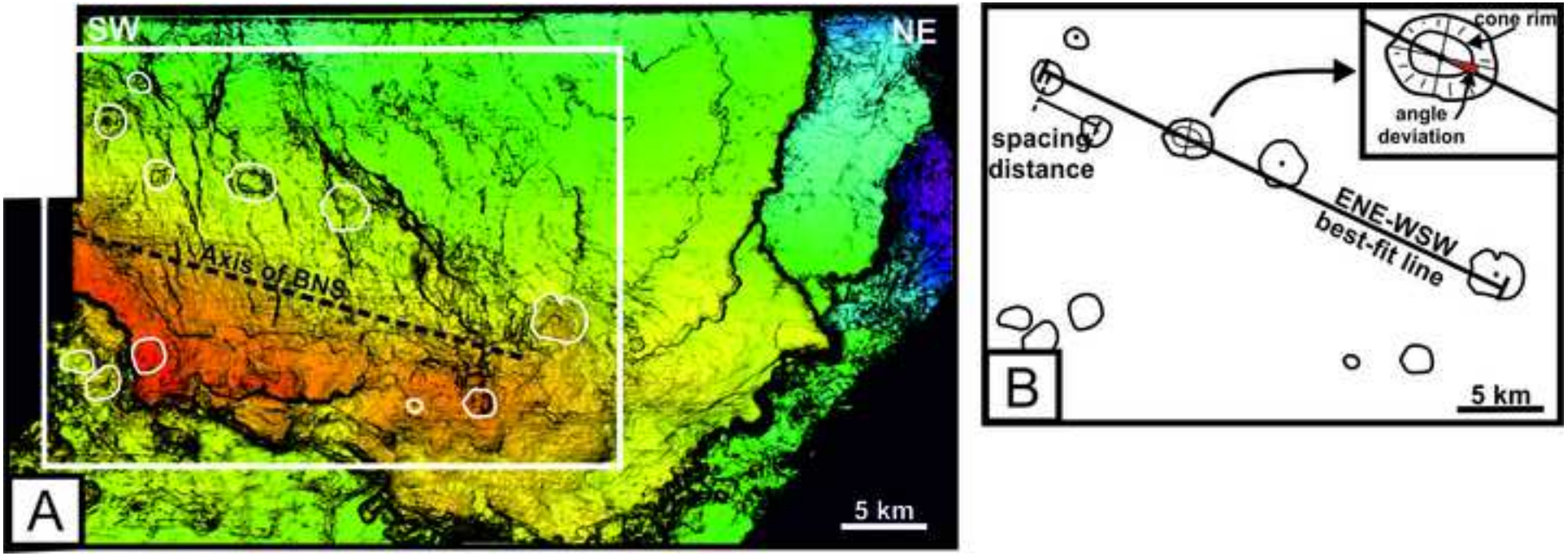

Figure 11

Click here to download Figure Figure 11.jpg

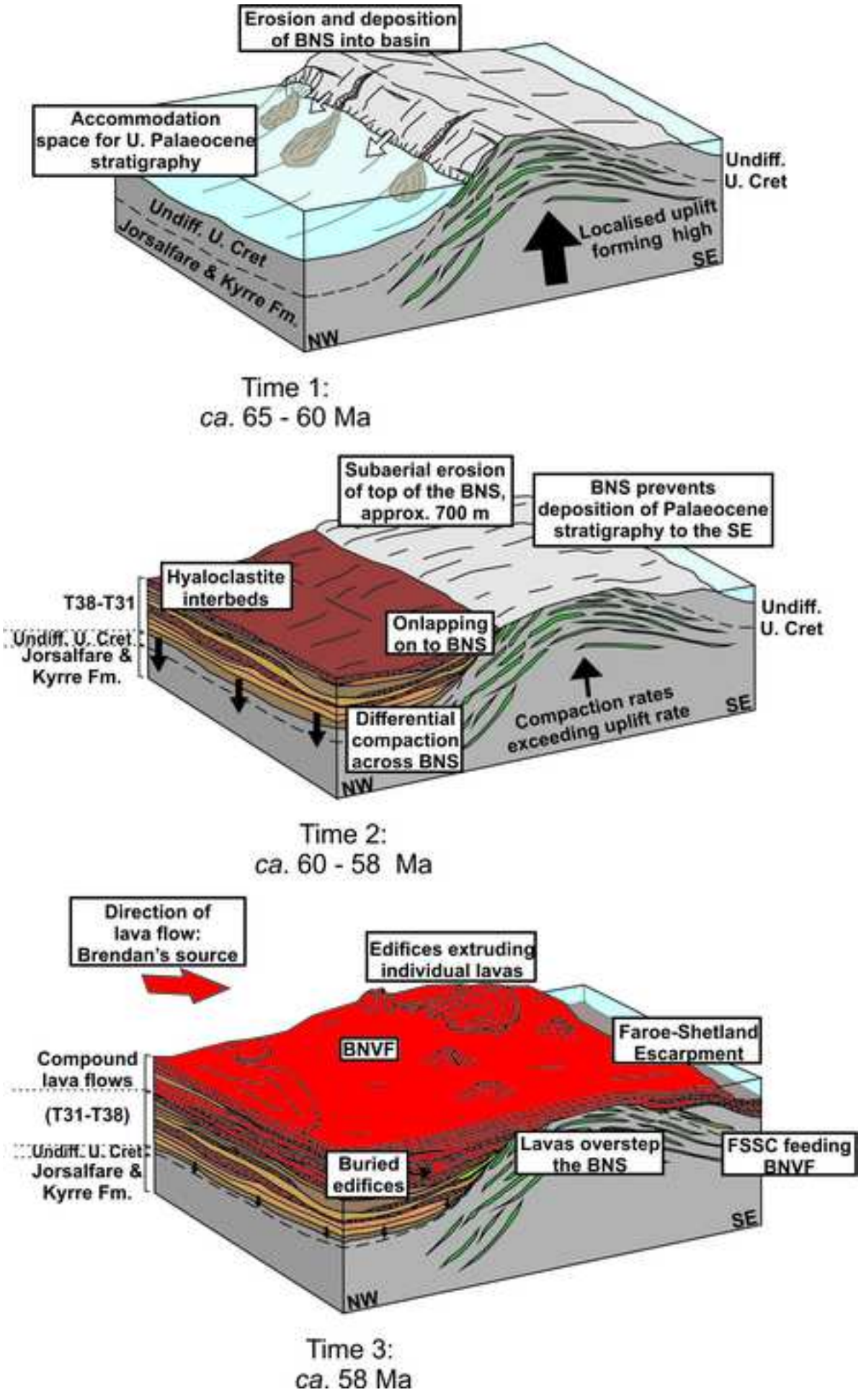

Figure 12

Click here to download Figure Figure 12.jpg

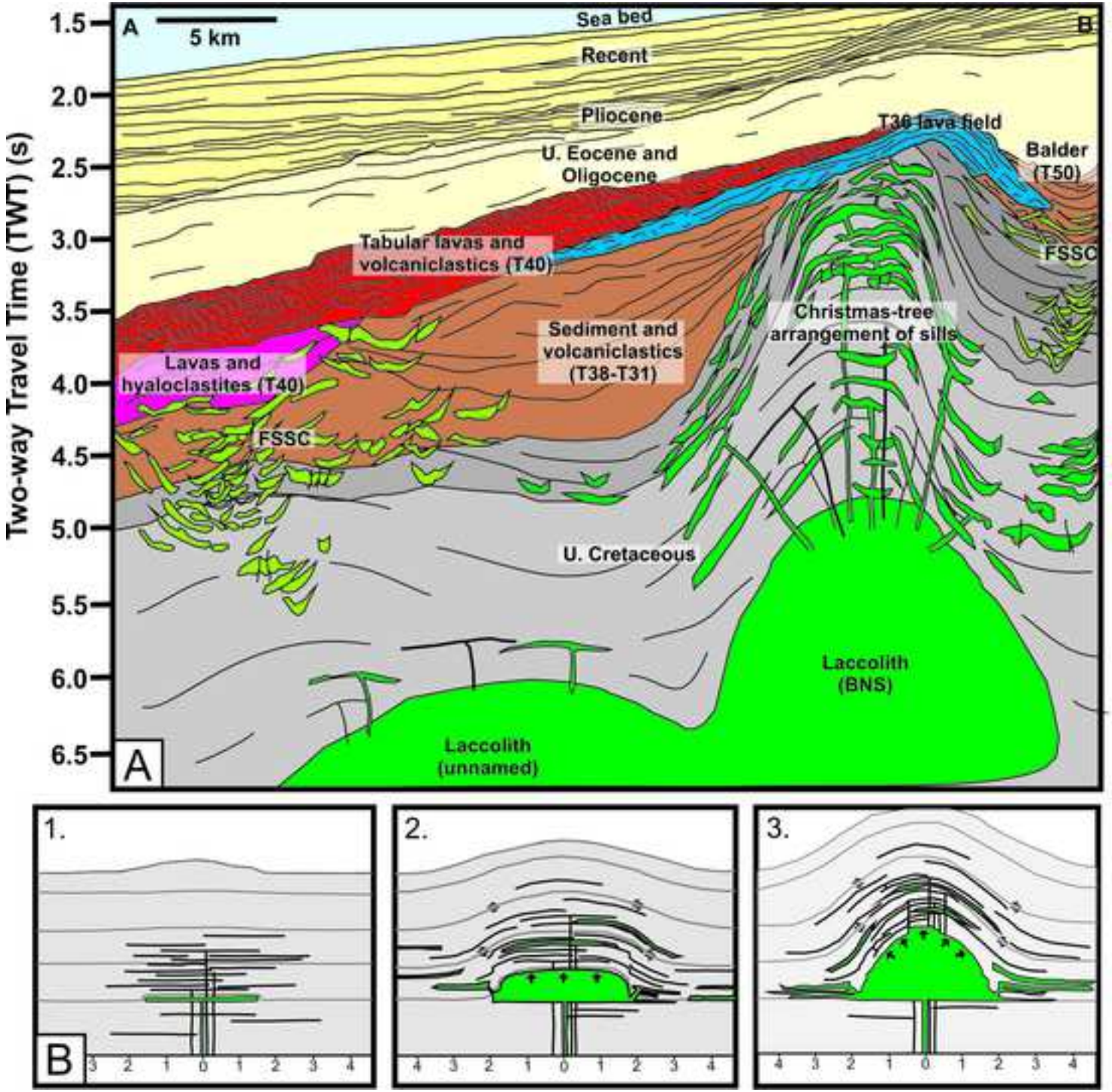

Figure 13

Click here to download Figure Figure 13.jpg

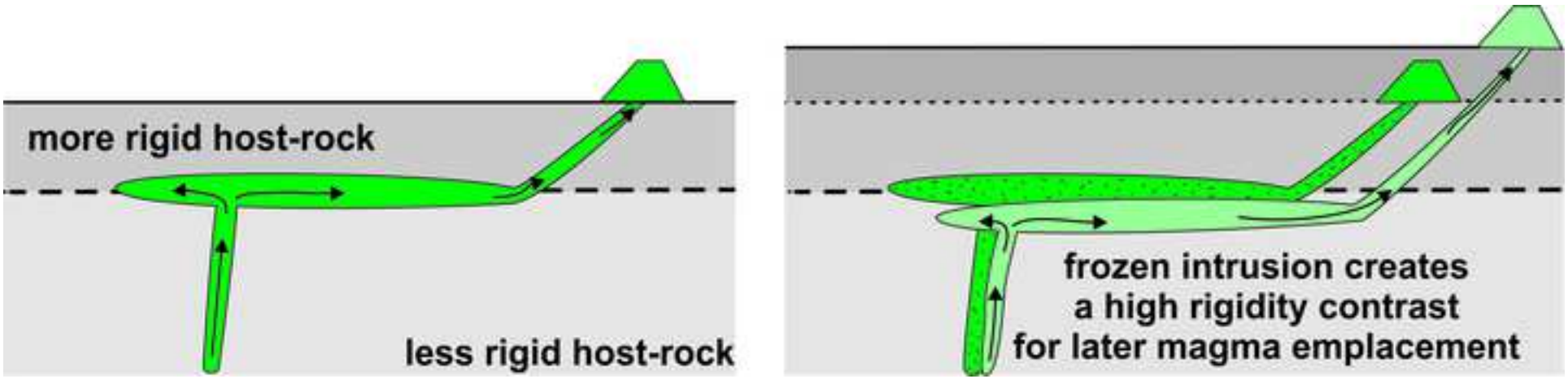

Figure 14

Click here to download Figure Figure 14.jpg

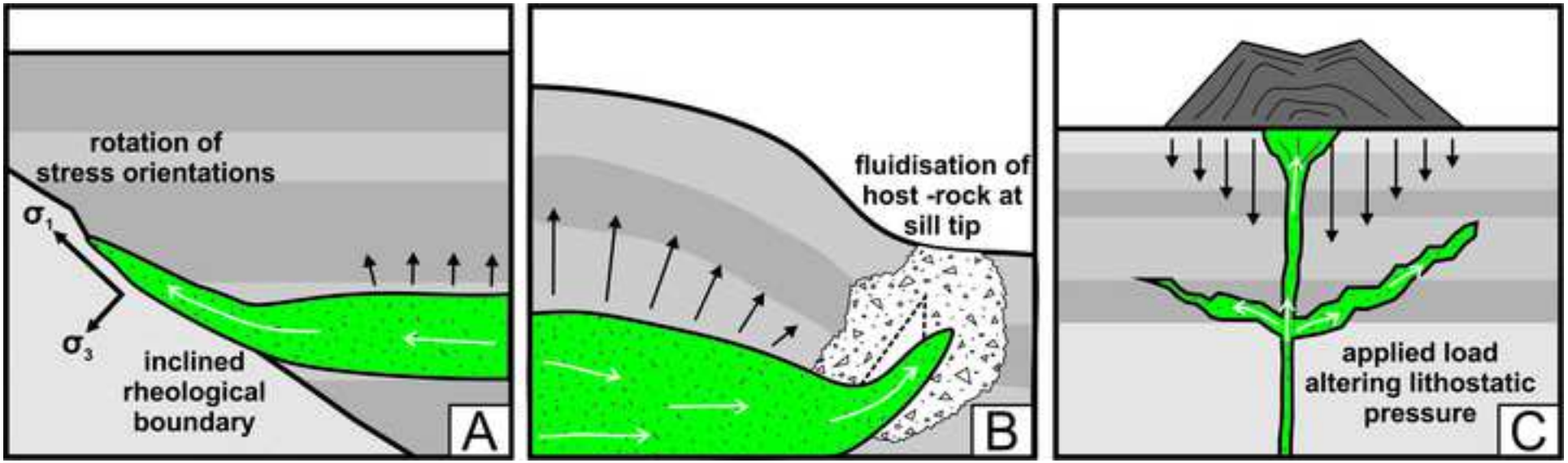

Click here to access/download

Supplementary material (not datasets)

supplementary data.xlsx